ADVANCED OPTICAL MATERIALS
www.advopticalmat.de

Physics and Applications of High-β Micro- and Nanolasers

*Hui Deng, Gian Luca Lippi, Jesper Mørk, Jan Wiersig, and Stephan Reitzenstein**

Micro- and nanolasers are emerging optoelectronic components with many properties still to be explored and understood. On the one hand, they make it possible to address fundamental physical questions in the border area between classical physics and quantum physics, on the other hand, they open up new application perspectives in many areas of photonics. This progress report provides an overview of the exciting developments from conventional semiconductor lasers toward nanoscale lasers, whose function relies on increased light–matter interaction in low-mode-volume resonators and unconventional gain concepts. The latest advances in the physical understanding of light emission from high-β lasers, in which a large part of the spontaneous emission is coupled into the laser mode, are highlighted. In the limit of $\beta = 1$, this leads to thresholdless lasing and it is shown that quantum optical characterization is required to fully explore the underlying emission processes. In addition, emerging nanolaser concepts based on Fano resonators, topological photonics, and 2D materials are presented. Open questions, future prospects, and application scenarios of high-β lasers in integrated photonics, quantum nanophotonics, and neuromorphic computing are discussed.

1. Introduction

The revolutionary development of conventional semiconductor lasers toward micro- and nanolasers has made it possible in the past few years to explore the ultimate physical limits of these photonic devices.[1,2] Above all, the significantly increased light–matter interaction strength, in resonators with low mode volumes in the range of the cube-wavelength, allows micro- and nanolasers to break new ground. For example, the effects of cavity quantum electrodynamics (cQED) open up the possibility of realizing lasers that are based mainly on the gain of a single quantum emitter.[3] In addition, optical resonators with a low mode volume and high quality (Q)-factor also ensure efficient control of the spontaneous emission of the integrated gain medium. The Purcell effect or suitable mode engineering makes it possible to couple spontaneously emitted photons with high probability into the laser mode. This important process in micro- and nanolasers is quantified in terms of the β-factor which describes the fraction of spontaneous emission that is coupled into the considered laser mode.[4] The physical limit is reached for $\beta = 1$, the so-called thresholdless laser.[5] In addition to the exciting physics of high-β lasers, these devices are also extremely interesting for energy-efficient applications, since the lasing threshold can be reduced by orders of magnitude.

In this progress report, we present an overview of the current state of development of high-β micro- and nanolasers and discuss open questions as well as future challenges and prospects for these exciting devices. The addressed topics include the latest investigations of small scale vertical-cavity surface-emitting lasers (VCSELs) in the limit of the smallest light intensities at the laser threshold in Section 2, where the description of the emission processes using semiclassical rate equations reaches its limits and stochastic methods are required for successful modeling. Building on this, Section 3 presents the fundamentals and current developments in high-β lasers leading to the "holy grail" of laser physics: the thresholdless laser. In this context, we review the challenges in characterizing high-β devices and emphasize the need for quantum optical measurement methods for the clear identification of coherent light emission. An interesting sub-class is represented by bimodal microlasers, where coupling through the gain medium leads to intriguing effects such as super-thermal light emission and unconventional normal mode coupling (Section 4). Looking beyond conventional devices, emerging nanolaser concepts are discussed in

Prof. H. Deng
Department of Physics
University of Michigan
Ann Arbor, MI 48109-1040, USA
Prof. G. L. Lippi
Université Côte d'Azur, Institut de Physique de Nice (INPHYNI)
UMR 7010 CNRS
1361 Route des Lucioles, Valbonne F-06560, France
Prof. J. Mørk
DTU Fotonik
Technical University of Denmark
Kongens Lyngby DK-2800, Denmark
Prof. J. Wiersig
Institut für Physik
Otto-von-Guericke-Universität Magdeburg
Postfach 4120, Universitätsplatz 2, D-39016 Magdeburg, Germany
Prof. S. Reitzenstein
Institut für Festkörperphysik
Technische Universität Berlin
Hardenbergstraße 36, 10623 Berlin, Germany
E-mail: stephan.reitzenstein@physik.tu-berlin.de
The ORCID identification number(s) for the author(s) of this article can be found under https://doi.org/10.1002/adom.202100415.

DOI: 10.1002/adom.202100415

Section 5, providing an outlook on realizations with great development potential. On the one hand, Fano lasers, based on very interesting physics, are particularly attractive for ultra-fast on-chip applications. On the other hand, topological lasers and new devices based on novel 2D gain materials open up entirely new perspectives. Interestingly, work on high-β lasers has focused on technological development and on the study of their emission properties. Only recently have the first "real" applications been conceptually suggested and experimentally demonstrated. Before offering a short conclusion, we thus highlight (Section 6) this important aspect of nanolasers, stressing their high application potential in the field of optical interconnects, in quantum nanophotonics, and in optical neuromorphic computing.

2. Exploring the Limits of Small Scale VCSELs at Low Light Levels

The exploration of laser physics at the microscale[6,7] can be traced back to the quest for reduced cavity volume,[8–15] well-discussed in an early review,[16] and to the consequent technological benefits coming from improved efficiency, reduced thermal load, and smaller footprint in telecommunications. Concomitant work on spontaneous emission in atomic physics[17–23] provided the support for the early development of dye microlasers[24–27] and of VCSELs.[28–32] Cavity engineering, based on the Purcell effect,[33–35] enabled the construction of resonators where the β-factor is increased,[36,37] as discussed in more detail in Section 3. At this scale, however, the standard Maxwell–Bloch laser description,[38–40] excellent for modeling macroscopic lasers, fails because it neglects spontaneous emission. For micro- and nanolasers comprising a single or a few emitters in the active region, it is feasible to solve full quantum mechanical models of the laser dynamics.[41–43] Such models show the intricate transition from below-threshold operation featuring dressed states to the emergence of a single dominant peak in the lasing region.[41] For microlasers with extended gain media comprising many emitters, rate equations have been tremendously successful.[44] In these, the fraction of spontaneous emission feeding into the photon population of the lasing cavity mode is explicitly taken into account. It was shown that the photon number predicted by properly derived effective rate equations agrees quantitatively with the outcome of full quantum mechanical models, below as well as above threshold.[43] The inclusion of spontaneous emission in the rate equations enables the description of the below-threshold regime and the smooth growth of the emission as a function of growing pump power,[31] but it leads to questioning the concept of laser threshold, best illustrated by the paradoxical identification of the $\beta = 1$ case with a thresholdless.[45,46] or zero threshold laser[25] (see Section 3). Although the $\beta = 1$ case provides a strictly linear input-output laser response only in the absence of non-radiative losses (cf.[29] for a rate-equation based proof and[47,48] for photoluminescent measurements), it represents a sufficient reason for calling into question the principle of lasing threshold.

Aside from niche technological applications, micro-VCSELs have become today the main source of information on the physical interaction between electromagnetic field and emitters. Their privileged bridging position between the macro- and the nanoscale, enables a sufficiently detailed analysis of the physics of light–matter interaction. **Figure 1** offers a synopsis of the evolution (top arrow) from the macro- to the nanoscale with the accompanying level of model description. The distinction among the three scales is qualitative and can be best pictured on the basis of (inverse) cavity volume (V^{-1}), as a surrogate for several indicators which quantify the device's characteristics (β-factor, Purcell factor and cavity Q-factor[49]). One way of loosely quantifying a border between scales makes use of the relative fluctuations at threshold as defined on the basis of a quantum statistical theory of the laser.[50] Thus, microscopic devices (or mesolasers) are characterized by $10^{-4} \leq \beta \leq 10^{-2}$, followed by nanolasers $\beta \leq 1$.[51] Macroscopic devices ($\beta < 10^{-4}$) are a good approximation of a thermodynamic optical system, which ideally requires an infinite number of electromagnetic cavity modes. The large-size system description satisfactorily describes the laser threshold as a second-order phase transition,[52–55] thus occurring at a precise value of the pump rate (control parameter). Here, radiation changes its nature from entirely incoherent to purely coherent at a precise pump rate value (in practice over a negligibly small interval), thus masking any possible intermediate steps in the evolution of the light–matter interaction. At the extreme nanoscale end, on the other hand, the interaction is best described quantum-mechanically, as long as the number of emitters and modes involved in the interaction is small (typically less than 10). Presently, technological constraints related to the responsivity of fast detectors strongly limit its investigation to mostly statistical properties of the emission. The intermediate, very extended range presents features of finite-size systems and benefits from a stochastic description, stemming from the discreteness of the physical processes which characterize the exchange between emitter excitations and photons, and from the impossibility of considering large size averages. While microlasers also cover part of this intermediate scale range, nanolasers represent the hinge which bridges the gap between the two extreme regimes. In particular, they marry a larger photon flux—improving the experimental accessibility to information—to surviving finite-size features, in addition to a broader pump range interval over

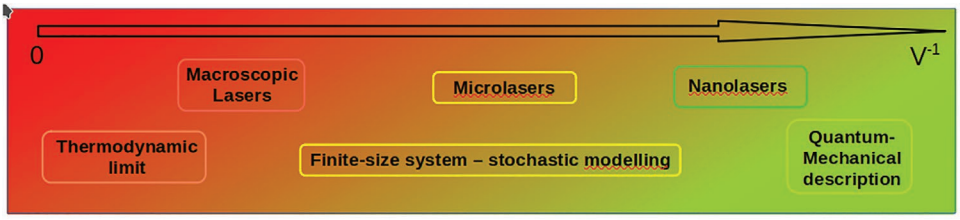

Figure 1. Graphical illustration of the transition from macroscopic to nanolasers with accompanying physical characteristics.

which the threshold is stretched. This unique and fortunate combination of attributes enables the detailed observation of the evolution of the interaction between radiation and matter on the way toward lasing.

A two-level micromaser with strong coupling to a single cavity mode [11] emits coherent light even at the lowest power levels (fraction of a photon present in the cavity, in average). This remarkable configuration, however, does not shed useful light onto the much more complex laser behavior [37], where the questions raised by the smoothness of the transition between incoherent and coherent emission in small-sized devices [32, 38, 39] still remain. Quantum statistical considerations[50] explain the origin of a threshold in the thermodynamic limit and of its disappearance at the micro- and nanoscale. Although conceptually correct, this result neither advances our understanding of micro- and nanolaser physics, nor does it offer practical advice for the realization of devices whose coherence properties must be ensured for applications (e.g., Mach–Zehnder-based all-optical operations for on-chip photonics[56,57]). Yet, since experimental evidence for Poissonian photon statistics exists even in nanolasers,[58–66] what is sorely missing is a fundamental understanding of the transition toward coherence: The simple collection of existing experimental observations leads indeed to an extremely complex and confusing picture. A practical approach used by micro-VCSEL manufacturers to circumvent the problem is to specify a *threshold current* high enough to ensure coherence (compare, e.g., ref. [67] with the measured response in ref. [68]). Although pragmatic, this approach does not answer the fundamental threshold question.

As mentioned above, micro-VCSELs ($\beta > 10^{-4}$ with an upper limit approaching 10^{-2}) represent an ideal compromise between the emergence of complex threshold physics—rather than a sudden transition—and the technological constraints which restrict nanolaser investigation to photon statistical measurements. Wide-bandwidth detectors (up to 10 GHz) have sensitivity as low as a μW, thus permitting time-resolved measurements with a photon flux about three orders of magnitude below the lasing edge, or about one order of magnitude below the "standard threshold" defined in ref. [50] for a $\beta = 10^{-4}$ laser. This performance enables the collection of a complete set of data which can be analyzed with dynamical, as well as statistical indicators[68,69] offering a much better set of tools to characterize the laser dynamics during the transition between incoherent and coherent emission. In addition, fast oscilloscopes with large memory depth permit the collection of very large datasets over sufficiently short time intervals to ensure good experiment stability. The commercial availability of a number of robust and durable devices with different characteristics eases the technological side of the investigations, without excluding the realization of custom-made samples.

Although the great potential of optical microcavities was already seen in the early 1990s[70] and experimentally some threshold properties were observed (in micro-VCSELs,[31,71,72] as well as in microdisk lasers[73,74]), most of the early reports focused on obtaining ever decreasing pump power and coherence properties. At the end of the 1990s, detection systems were not as advanced as to allow the good characterization that we can now obtain, thus fundamental work on microlasers was vigorously pursued on custom-built solid-state microlasers with "relatively high" β-factors ($\approx 10^{-5}$).[75] Although some of the conclusions reached at the time[76] have been recently revised in light of micro-VCSEL measurements[51] and models,[77] these surrogate investigations allowed for conceptual inroads into nanolaser threshold physics and represent the first major contribution in establishing connections across laser scales.[78]

More recent micro-VCSEL experimental contributions to the description of the transition from incoherent to coherent laser emission come from experimental evidence which can be summarized as follows. The observed smooth transition, in the average laser response, hides a wealth of information on the physics which develops in the various stages.[68] The first observation is the appearance of photon bursts which precede the establishment of a continuous coherent field. These bursts, easily obtained also with the stochastic simulations (cf. discussion below) and interpretable on the basis of topological considerations,[79] had not been previously reported, but indirect traces can be found in the nonzero average, below-threshold oscillation of two orthogonal polarizations.[72] Their features are illustrated in **Figure 2**a,b which shows the stochastically computed bursts for a $\beta = 10^{-4}$ (a) and $\beta = 10^{-3}$ (b) laser. Their

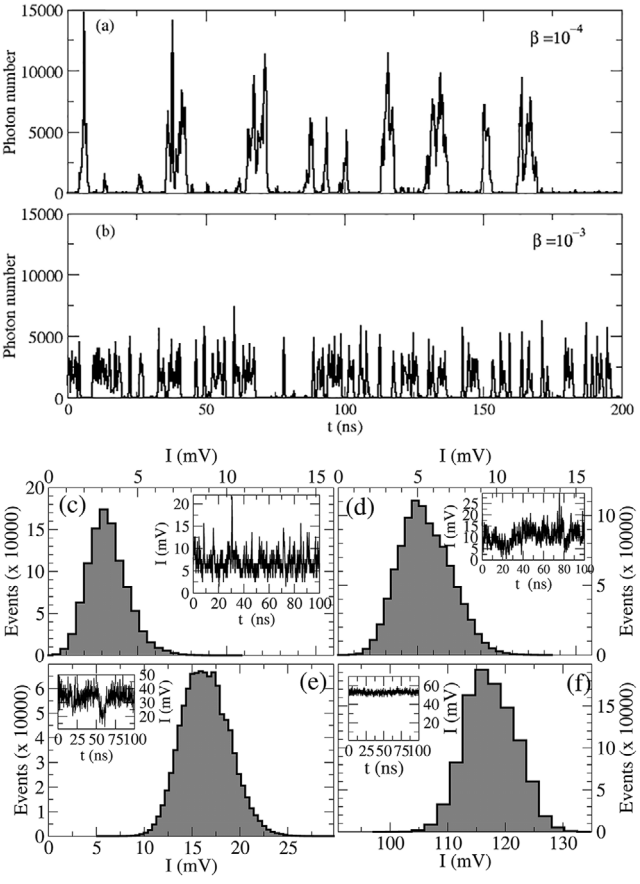

Figure 2. a,b) Stochastically computed photon bursts for microlasers with different β-factor (adapted with permission from Figure 7 of ref. [51], Copyright 2020, American Physical Society). c–f) Experimental PDF and sample traces (insets) obtained from measurements in a micro-VCSEL (adapted with permission from Figure 4 of ref. [51], Copyright 2020, American Physical Society). The injected current values are $i = 1.26$ mA (c), 1.30 mA (d), 1.45 mA (e), and 3.0 mA (f). "Threshold" is estimated to be close to the injection current of panel (e).

main feature is a peak amplitude which can be more than two orders of magnitude larger than the average photon flux ($\beta = 10^{-4}$), with frequency (and shape) which increase at the expense of amplitude as β grows.

Up until now, aside from micro-VCSELs, no other system probably possesses the needed stability, and a sufficiently broad pump interval over which the photon bursts appear, to allow for their systematic observation. The height and frequency of the bursts can give rise to strong photon bunching with superthermal statistical properties[51] in the single-mode regime. The frequency of the photon bunches increases, while their height (photon number) decreases, to eventually give rise to an initially strongly noisy continuous-wave (cw) coherent laser emission. The experimentally measured probability density function (PDF) shown in Figure 2c–f illustrates the evolution through the threshold region starting from below threshold.[68] Panel (c) shows a peaked PDF—measured below threshold—with a long tail at large photon numbers, which matches the spikes exemplified in the corresponding inset (photon burst—only the tip is visible due to the detector sensitivity; electrical noise ranges between approximately 5 and 8 mV). This PDF strongly differs from the one of macroscopic lasers below threshold.[80] As the current injection increases (remaining below threshold) the PDF deforms (panel (d)) to something more symmetrical, due to a burst amplitude reduction and frequency increase, which start forming an irregular signal (inset of panel (d)), to eventually give rise to only occasional drops of power to the noise level (PDF of panel (e), with a power drop illustrated in the inset). Finally, a PDF compatible with regular lasing appears in panel (f). It is interesting to notice that true lasing (i.e., the photon statistics is well described by Poisson statistics) lies well beyond the manufacturer-specified threshold[67] (typical specified threshold current $i_{th} = 2.2$ mA with maximum 3 mA), at least for the devices that were studied[68] (Poisson statistics reached at $i_{th} \approx 4.5$ mA[51]). The second-order zero-delay autocorrelation function for the photon number n

$$g^{(2)}(0) = \frac{\langle n^2 \rangle - \langle n \rangle}{\langle n \rangle^2} \tag{1}$$

shows plateaus of (nearly) constant autocorrelation,[68] whose origin can be reconduced to a complex dynamical interaction between carrier density (i.e., the energy reservoir) and the photon field. It is interesting to notice that similar structures have recently been observed in a metallic nanolaser.[81] While the complex procedure to reconstruct the autocorrelation may induce one to think that not too much weight should be placed on this resemblance, it is nonetheless worth pointing out the similarities, for a purely random likeness seems improbable. Further work is needed to prove whether the route observed in the micro-VCSEL[68] extends to nanolasers as well.

The resulting understanding of the threshold region's structure and of the transition between photon bursts and cw oscillation has enabled the establishment of a technique for experimentally identifying lasing.[82] It is based on a modulation of the pump current with a frequency close to the inverse of the typical repetition rate of the photon bursts before the transition to cw operation.[83] The latter precedes the emergence of the well-known relaxation oscillations, which only exist in the presence of the coherent field. A resonance between the modulation and the photon emission is detected by the autocorrelation function. Numerical predictions show that, although less pronounced, the effect holds for nanolasers and should provide a simple experimental technique for detecting the onset of cw, superpoissonian (weakly) coherent emission[82] as a possible alternative to quantum optical studies on the photon statistics of emission (see Section 3).

The improved insights into the threshold physics at the microlaser scale have suggested the possibility for alternative information encoding schemes, with lower power consumption and without changes in device construction, where reasonably regular photon bursts can be induced near threshold.[84] Similarly, trains of photon bursts, with increased regularity, appear thanks to optical feedback when a micro-VCSEL is biased close to its threshold.[85]

Although current efforts are mostly devoted to nanolaser development, as detailed in the following sections, a great deal of attention is currently being paid to the technological applications of micro-VCSELs, especially in the telecom sector. High-speed, low-energy consumption devices have been developed over the past decade[86–89] for high-speed modulation and optical link implementation, extensively reviewed in.[90] Similarly, VCSEL designs, although not capable of providing true nanolaser characteristics, continue to attract attention in the development of small sources.[91] An extensive reference list can be found in ref. [92].

A number of the previous observations have been guided and/or explained with the help of a fully stochastic modeling approach, a necessary support for providing a fundamental understanding of the transition between incoherent and coherent emission. The model is based on Einstein's semiclassical theory for the interaction between radiation and matter[93] and has been implemented into different schemes, for example, in ref. [94,95] (after a proposal in[50]), and in ref. [96] (following previous work[97]), both using a Monte Carlo approach; in ref. [98] as a discretization of rate equations; and in ref. [99–101] on individual trajectories over which averages are then taken. All physical processes (pump, absorption, emission—both spontaneous and stimulated—, and photon transmission through the cavity mirror) are evaluated as probabilistic events which involve integer number of exchanges (photons and excitation). Thus, not only are the times at which each process occurs random—as well as the number of events—but the discreteness introduces a granularity which differentiates it substantially from the differential representation[98] and gives rise to intrinsic noise, which is otherwise introduced as a Langevin process in continuous models. The mostly numerical predictive power stems from the intrinsic granularity in time and events (photons and excitations) which automatically account for a poissonian "noise". Quantities can be computed to match experimental observations and provide predictions in excellent agreement with the observations.[102]

The physical meaning of the photon bursts is not yet entirely clarified, but may play a conceptually fundamental role in the establishment of coherence. Photon-statistical work on early lasers[80,103] established that the transition between incoherent and coherent emission takes place through a statistical mixture

of the two kinds of radiations.[102] Photon bursts may enlarge the picture by describing the temporal evolution which was summarized in those statistical considerations.[102]

To conclude this section, it is important to remark the appearance of a new model (extending work aimed at the description of semiconductor-based nanolasers[104–108]) which—at variance with rate equations — introduces the incoherent and coherent field as separate variables, and univocally identifies the position of the growth of the coherent component through a bifurcation analysis.[109] This picture provides the first clear definition of the laser threshold, regardless of laser size and solves the problem raised by the rate-equation picture,[4,45,110] circumventing the thermodynamical constraints which prevent the identification of a threshold in small systems.[50]

3. Ultra-High-β Nanolasers: Entering the Thresholdless Lasing Regime

A significant impetus for the development of micro- and nanolasers, beyond the small scale VCSELs discussion of the previous section, was and is still provided by the perspective of realizing lasers with high β-factors. With regard to possible applications, this opens up the opportunity for reducing the laser threshold by orders of magnitude,[111] thus increasing the lasers' energy efficiency. In addition, high-β lasers can be used to explore the thresholdless lasing regime, which is extremely interesting from a fundamental point of view. In the following, current developments from high-β lasers to the regime of thresholdless lasing are presented and discussed in this context.

3.1. The Foundations and Development of High-β Lasers

Research in high-β lasers, including the thresholdless case, dates back to the beginning of the 1990, as already mentioned. On the basis of experimental results in a microcavity[25] and early rate-equation modeling,[45] Bjork, Karlsson, and Yamamoto in 1994 dealt with the question of a suitable definition of the laser threshold of microlasers.[111] In the extreme case of one unique cavity mode resonating with the gain medium, no threshold can be identified on the basis of the output characteristics as the latter is a straight line, whence the term "thresholdless". This early work, however, identified the need for a finite amount of pump to achieve coherent laser emission, based on the requirement of at least one photon in the lasing mode (on average)[111] to reach threshold, thus already invalidating the "zero-threshold" denomination. Furthermore, an analysis of the quantum Langevin rate equations showed that the threshold pump value would be reduced by orders of magnitude, going from macroscopic ($\beta < 10^{-4}$) to thresholdless devices ($\beta = 1$) and that in the latter, lasing could occur without population inversion. The β-factor itself can be influenced by cQED effects and in micropillar resonators can be expressed, through an effective Purcell factor F_P, by $\beta \approx F_P/(F_P + 1)$, that is, taking into account the contributions from all emitters.[112] The further proportionality $F_P \propto Q/V_{\mathrm{mode}}$ directly relates β to the Q-factor and, inversely, to the mode volume V_{mode}. The latter expression explains the great scientific interest in laser resonators with high-Q and low-volume modes to decrease the threshold pump power and to enter the regime of thresholdless lasing. We would like to note that the impact of the Purcell Factor, the Q-factor, and the β-factor are discussed in detail in a recent review article dedicated to the memory of M. I. Stockman.[113]

Based on the enthusiasm arising from early theoretical work on high-β lasers, great technological efforts were directed at manufacturing and experimentally investigating such devices, with major advances, at the turn of the millennium, especially in the area of quantum dot (QD)-based microlasers. High-β lasing was demonstrated in QD microdisks,[74,114] QD micropillars,[115] and also in QD photonic crystal (PhC) cavities,[58,116] with the latter reaching a β-factor up to 0.85. It is interesting to note that the underlying technological advances in resonator fabrication also enabled the investigation of single-QD lasing effects in microdisks,[117] micropillar cavities,[118] and PhC cavities[3] in the cQED regime of weak coupling and later also in regime of strong coupling in PhC cavities[119] and micropillars.[120]

Plasmonic nanolasers[2] constitute a different interesting class of devices where light is confined—at least partly—by a metallic mirror. As a result, the modal volume can be substantially restricted to values even well below the cubic wavelength of the emitted light. Typically, the gain medium consists of a 3D semiconductor material or of 2D multiple quantum wells (QWs). Prominent representatives of this class are nanolasers based on a metal-insulator-semiconductor-insulator-metal plasmonic gap mode[121] and plasmonic nanolaser based on a two-dimensionally confined nanowire plasmonic mode[122] with a β-factor of up to 80%.

The first thresholdless semiconductor laser was demonstrated in 2012.[5] It is a so-called coaxial nanolaser with a QW gain medium. In this type of plasmonic nanolaser with dimensions of a few 100 nm, the mode confinement is implemented, as shown in the inset of **Figure 3**a, via a central rod surrounded by the semiconductor gain medium with a metallic outer shell. A SiO_2 plug between the upper part of the semiconductor and the metallic resonator prevents the creation of undesired (dissipating) plasmonic modes. Optical excitation and emission take place via the lower opening of the resonator. Due to the small mode volume of the coaxial nanolaser (ideally) only one resonator mode overlaps with the gain medium, which here consists of six InGaAsP QWs. This, together with a moderately high Q-factor (in the range of 200–300), promises a β-factor of 0.99 and, accordingly, virtually thresholdless lasing. The experimental data (red dots), which are shown in Figure 3a for a measurement with optical excitation at 4.5 K, confirm the ultrahigh β-factor and the virtually threshold-free lasing behavior. In fact, the output power here rises almost linearly with the input pump power, as indicated by the blue line. Figure 3b shows the corresponding linewidth of the emission at a wavelength of 1.5 μm as a function of the pump power. The power-dependent decrease in the linewidth above about 2×10^{-7} W, which corresponds to the threshold pump power of this laser, indicates the transition from spontaneous to stimulated emission with increased temporal coherence. This behavior also illustrates the aforementioned point that a thresholdless laser also needs a finite pumping power to produce laser emission.

After this milestone result, (near) thresholdless lasing was also achieved in other resonator types and gain configurations.

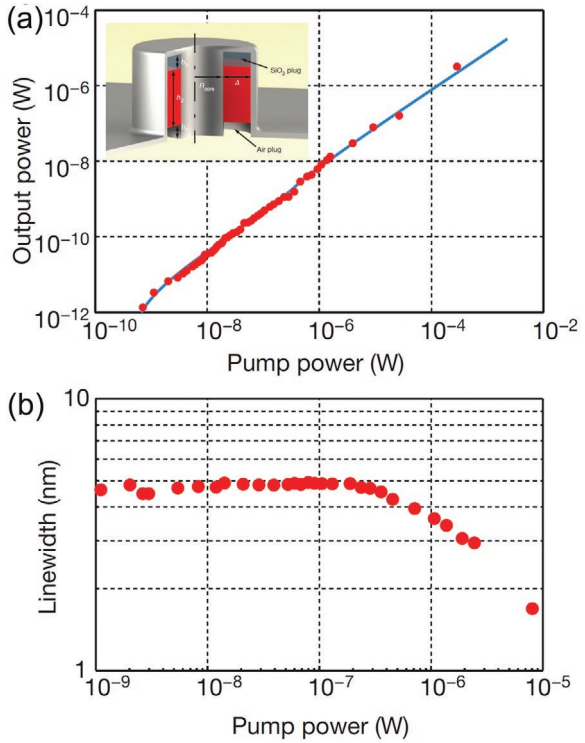

Figure 3. Thresholdless coaxial nanolaser. a) Input–output characteristics of coaxial nanolaser with a gain medium composed of six InGaAsP QWs at 4.5 K. The linear power dependence (indicated by the blue line) is characteristic for the thresholdless operation of the laser. As shown in the inset, the coaxial resonator consists of a metallic (silver) rod which is enclosed by a metal coated semiconductor ring. Typical dimensions are $r = 100 - 200$ nm and $\Delta = 75 - 100$ nm. b) Corresponding dependence of the emission linewidth. The decrease of linewidth for pump power values above 10^{-7} W indicates the transition from spontaneous emission to stimulated emission with enhanced temporal coherence. Adapted with permission.[5] Copyright 2012, Springer Nature.

This includes demonstrations in PhC cavities with buried QW gain medium[123] and InGaAs QDs[124] at cryogenic temperature, and laser demonstration at room temperature in PhC cavities with InAsSb QDs[125] and GaN nanobeam cavities with an InGaN/GaN QW.[126] These advances in the field of high-β lasers have initiated a vivid debate about the emission properties that characterize a thresholdless laser and how laser operation can be clearly demonstrated in such a laser. This aspect is discussed in the following section.

3.2. How to Verify High-β and Thresholdless Lasing?

In conventional semiconductor lasers, the detection of the laser emission is usually done by simply recording the input-output characteristic, whereby the transition from spontaneous to stimulated emission at the laser threshold is clearly noticeable in a pronounced non-linearity. In addition, the increased temporal coherence of lasing emission above threshold shows the characteristic P^{-1} dependence, where P is the optical power, of the linewidth reduction predicted by Schawlow and Townes.[127]

In contrast, it is difficult (impossible) in high β (thresholdless) lasers to determine the transition to stimulated emission via the input-output characteristic. A lively debate around lasing characterization in high-β devices proved that linewidth reduction is usually insufficient to prove lasing.[110] Against this background, the quantum optical measurement of the emission statistics has established itself in recent years as proof of laser operation in high-β micro- and nanolasers.[1,58–60,62,119]

We now discuss the correct and unambiguous detection of laser emission in high-β devices, pointing out possible pitfalls in the interpretation of experimental data. A family of microresonators with different optical amplification and otherwise very similar optical properties lends itself to this discussion.[63] The selected structures are AlGaAs/GaAs micropillar cavities with a single active layer of InGaAs QDs. The number of QDs effectively coupled to the relevant optical mode can be controlled through the pillar diameter (here between 2.0 and 2.5 µm) and the position in the wafer. Operation of each device either as a laser or a LED, emitting photons exclusively spontaneously, can be mastered this way.

In the present case, three QD micropillars, A, B, and C, with a diameter of 2.0, 2.0, and 2.5 µm, respectively, were selected and their emission was examined. The corresponding input–output characteristics are shown in **Figure 4**a. Here, the ordinate shows

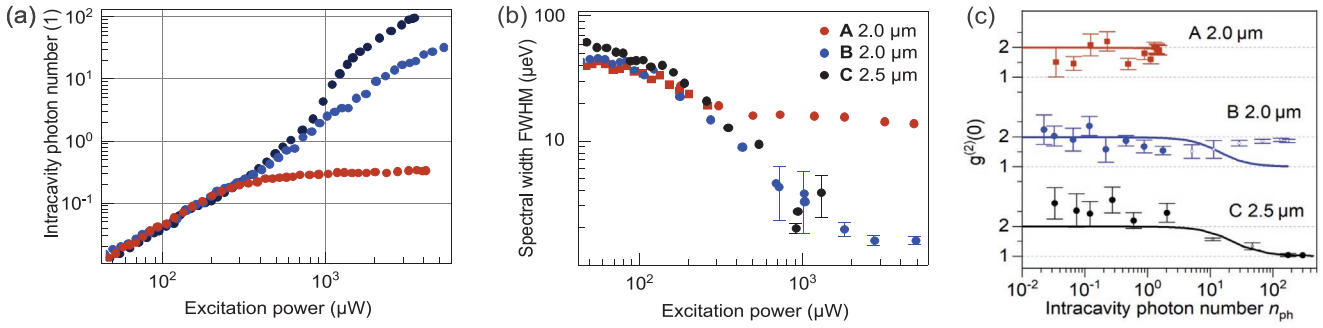

Figure 4. Emission properties of a family of optically pumped QD micropillars with a diameter of 2.0 µm (pillar A and B) and 2.5 µm (pillar C), respectively. a) Input-output characteristics indicating LED-like behavior for pillar A, high-β lasing for pillar C, and possibly thresholdless lasing operation for pillar B. b) Corresponding emission linewidth as function of excitation power. c) Photon autocorrelation function at zero time delay $g^{(2)}(0)$ as function of intracavity photon number for the three considered micropillars A, B, C. The measured $g^{(2)}(0)$ values indicate LED-like behavior for micropillar A, high-β lasing for micropillar C, and cavity enhanced thermal emission for micropillar B. Adapted with permission.[63] Copyright 2017, Springer Nature.

the intracavity photon number, n_{Ph}, determined via a theoretical modeling of the experimental characteristics. The optical gain of microresonator A is not large enough to reach the threshold ($n_{Ph} = 1$) for laser emission; the intracavity photon number saturates therefore at $n_{Ph} \approx 0.5$. Consistent with this finding, the emission linewidth (panel (b)) decreases only slightly over the considered pump power range, a reduction attributed to the saturation of optical absorption channels. In contrast, micropillar C shows an s-shaped power characteristic typical of a laser combined with n_{Ph} of up to 200, a laser threshold at about 600 μW (at $n_{Ph} = 1$), and a significant decrease in the emission linewidth, as shown in panel (b). The behavior of micropillar B is very interesting, as it has an almost linear performance characteristic together with a strong and almost identical decrease in linewidth compared to micropillar C. According to these criteria, this could be a thresholdless laser.

In order to substantiate this "classic" interpretation of the experimental data, quantum-optical studies of the emission statistics were carried out on the three micropillars. Corresponding measurements of the second-order autocorrelation function ($g^{(2)}(\tau)$) via a Hanbury-Brown and Twiss configuration provide important insight into the underlying emission processes. In particular, the value $g^{(2)}(\tau = 0)$ can be used to distinguish between thermal emission with $g^{(2)}(0) = 2$ and coherent emission with $g^{(2)}(0) = 1$.[128] The experimental $g^{(2)}(0)$ values are plotted in Figure 4c for the three considered microresonators as a function of the intracavity photon number. For the LED-like micropillar in the spontaneous emission regime, the autocorrelation remains, as expected, around 2. For micropillar C, there is a transition from thermal (below threshold) to coherent light (above threshold), as expected in a laser. In contrast, micropillar B—previously considered as a possible thresholdless laser—shows a slight decrease in autocorrelation, around $n_{Ph} = 1$, from its thermal value, $g^{(2)}(0) = 2$, to then return to the emission of (pure) thermal light ($g^{(2)}(0) = 2$) at larger photon numbers. We would like to note that in the thermal regime, the experimental $g^{(2)}(0)$ values are usually lower than expected from theory because of the limited time resolution of the used detectors.[58,59] For the data presented in Figure 4c, the Siegert relation, which links the normalized first-order correlation function to the second-order photon autocorrelation function, was applied to overcome this limitation.[63] Interestingly, superthermal bunching with $g^{(2)}(0) > 2$ is observed for micropillar C below threshold which can be attributed to superradiant emission.[129] Superthermal bunching can also occur above threshold pump power in bimodal cavities,[130] where it indicates temporal mode switching in (Section 4).

This analysis reveals that micropillar B is a thermal emitter, rather than a thresholdless laser, which, despite a high intracavity photon number, does not reach the lasing threshold. This evidence proves that photon statistics is essential, particularly for high-β devices, in determining the presence of lasing. Against this background, all experimental work on the development of high-β micro- and nanolasers should be backed up by power dependent measurements of the photon statistics, as recently done in refs. [81,124,126]. Even deeper insight into the photon statistics can be obtained with a photon number resolving detector, as it provides access to higher order photon correlations (see Section 4.4).

3.3. Open Questions and Prospects

The last two decades of developments in the field of high-β lasers have enabled the exploration of the physical limits of thresholdless and single-QD lasing, while exposing new questions which require further investigation. The prospect of single-QD lasing was first introduced in ref. [131] and discussed in an instructive way in ref. [132], where it was concluded that single-QD lasing could be possible in the good-cavity limit of weak coupling in which the emission linewidth of the resonator is smaller than that of the QD. Until now, this regime, which requires ultrahigh Q-factors, has not been realized in experiment, and attempts to demonstrate the single-QD lasing have been made in the boundary of the bad-cavity limit, for which the cavity has a higher linewidth than the emitter (see ref. [3,117–120]). In this bad-cavity limit, it has been shown that although the optical amplification in single-QD lasers was provided dominantly by a resonant emitter, the gain contribution from further nonresonant QDs is necessary to enter the lasing regime.[133] For a real single-QD laser, the question arises as to whether it can (only) function in the regime of strong cQED coupling and how lasing and the climbing the Jaynes–Cummings ladder differ. In the area of high-β single-QD lasers, deterministic fabrication technologies are interesting, since they permit a precise control of the position and number of the QDs in the laser's active area. The buried-stressor growth method is predestined for this objective. With this method, the number of QDs in the active medium can be set in the range of about 1–20 during growth,[65] which can pave the way for a systematic study of few-QD laser toward the thresholdless single-QD limit in the future. Thresholdless lasing was achieved with optical excitation and with conventional QW and QD material. In addition, 2D quantum materials are considered as active media for nanolasers[134] (see Section 5.3), and the question arises whether threshold-free lasing can also be achieved in such structures. From an application point of view, it will be interesting to develop thresholdless lasers under electrical excitation. Questions about the modulation bandwidth, energy efficiency and the possible integration of high-β and threshold-free lasers in optoelectronic circuits occupy a special place in the list of topics which need addressing.

4. Physics and Prospects of Bimodal Microlasers

Bimodal lasing is a well-known phenomenon in macroscopic lasers such as ring lasers[135,136] and VCSELs.[72] In the realm of microlasers and nanophotonics, micropillars are good candidates for bimodal lasing as a slight ellipticity of the cross section lifts the spectral degeneracy of the fundamental mode (see inset of **Figure 5**d) leading to two modes with orthogonal linear polarizations.[137,138] Bimodal microlasers also naturally emerge in the context of evanescently coupled microcavities supporting two supermodes.[139–141]

There are a number of intriguing effects in bimodal microlasers associated with mode competition for the limited available gain. This includes bistability and hysteresis,[139] superthermal light emission,[138] stochastic mode hopping,[130] unconventional normal-mode coupling,[142] spontaneous symmetry breaking,[143] and pump-power-driven mode switching.[140,144]

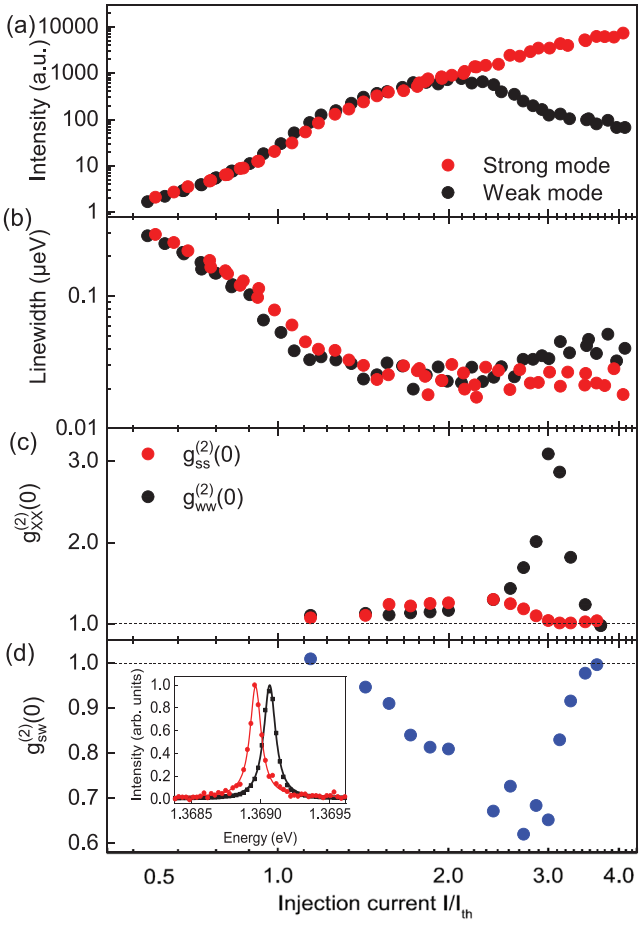

Figure 5. Measured characteristics of a bimodal $In_{0.3}Ga_{0.3}As$ QD-micropillar laser with a diameter of 3 μm and slightly elliptical cross section. The threshold current is estimated to be I_{th} = 5.1 μA. a) Input–output characteristic, b) emission mode linewidth and the photon c) auto- and d) crosscorrelation functions $g^{(2)}_{ss}(0)$, $g^{(2)}_{ww}(0)$, and $g^{(2)}_{sw}(0)$ of emission from the strong and the weak mode, respectively. The inset in (d) shows a polarization-resolved μEL emission spectrum. Adapted with permission.[138] Copyright 2013, American Physical Society.

4.1. Input–Output Characteristics and Intensity Fluctuations

A typical input–output curve of a bimodal microlaser is presented in Figure 5a. One mode (henceforth called the strong mode) exhibits an "s"-shaped input-output curve known from high-β single-mode microlasers (see Section 3 and Figure 4). In contrast, the intensity of the weak mode saturates and finally drops down for large injection currents. This mode loses the competition for the common gain material.

This interpretation is underpinned by the behavior of the linewidths in Figure 5b. Both linewidths first decrease dramatically due to the bleaching of the absorption of the active medium. While the linewidth of the strong mode stays at a resolution-limited value of about 25 μeV, indicating an enhanced temporal coherence due to stimulated emission, a slight increase of the linewidth can be observed for the weak mode above a current of three times the threshold current, indicating a growing contribution of spontaneous emission, but still, the linewidth is remarkably small.

The intensity fluctuations of bimodal lasers are described by the set of second-order equal-time correlation functions

$$g^{(2)}_{\xi\varsigma}(\tau=0)=\frac{\left\langle b^{\dagger}_{\xi}b^{\dagger}_{\varsigma}b_{\xi}b_{\varsigma}\right\rangle}{\left\langle b^{\dagger}_{\xi}b_{\xi}\right\rangle\left\langle b^{\dagger}_{\varsigma}b_{\varsigma}\right\rangle} \tag{2}$$

with ξ, ς = s, w, delay time τ, and photon annihilation operators b_s and b_w of the strong and weak mode, correspondingly. Figure 5c shows the HBT-setup measurement of the autocorrelation functions $g^{(2)}_{ss}(0)$ and $g^{(2)}_{ww}(0)$ as function of the injection current. Below threshold, the values of the autocorrelation functions are significantly below the expected value of 2 for thermal emission due to the limited temporal resolution of the HBT configuration.[59] Around threshold, $g^{(2)}_{ss}(0)$ shows a small maximum and approaches the value 1 for Poisson-distributed light, which indicates the transition from spontaneous emission to stimulated emission. In contrast, $g^{(2)}_{ww}(0)$ demonstrates a large maximum well above 2, proving superthermal emission. It is noteworthy that this superthermal light source is different from superthermal light sources based on sub- and superradiance (see, e.g., ref. [129]). Figure 5d shows that the crosscorrelation function $g^{(2)}_{sw}(0)$ exhibits a well-pronounced minimum, which is an evidence for a strong anticorrelation of the mode's intensities.

The experimental findings have been confirmed by full quantum calculations based on a microscopic semiconductor Hamiltonian[138] and by semiclassical calculations.[130] Both approaches support a two-state model:[130,138,145] In state 1, the strong mode is lasing with large intensity and the weak mode is nonlasing with relatively small intensity (not necessarily emitting thermal light[146]); in state 2, it is the other way round. This model is most intuitive in the semiclassical approach which predicts a mode hopping dynamics resulting from a dynamical bistability of the classical electric field subject to spontaneous emission noise.[130] The two-state model is an extension of the on–off model for macroscopic lasers (see, e.g., refs. [135,136]). The hopping dynamics and the laser characteristics can be controlled via selective optical injection into either the strong or the weak mode[147] or by time-delayed self-feedback.[148,149]

4.2. Unconventional Normal-Mode Coupling

Normal-mode coupling is an important topic in cQED. In the regime of strong (weak) coupling, the energies (linewidths) of the involved eigenmodes split. The indirect coupling of the two modes in a bimodal laser via the common gain medium can be understood as an unconventional normal-mode coupling.[142]

In the strong coupling regime, the eigenmodes of the total active system exhibit frequency locking (the well-known laser frequency locking), and the linewidths of the eigenmodes exhibit a splitting. On the contrary, in the weak coupling regime, the spectrum consists of two separated peaks with similar linewidths.[142] This explains the long coherence times of the weak mode observed experimentally in Figure 5b.

4.3. Mode Switching

Experiments on bimodal lasers have demonstrated a possible switching of the mode properties occurring when the pump power is increased beyond the laser threshold[140,144] (not seen in Figure 5a). This phenomenon is known from VCSELs as "polarization switching."[72]

At the switching point the intensity anticorrelation is most distinct, whereas the strongest bunching appears just before and after the switching point. For micropillar lasers, the effect has been discussed in terms of the competition between effective gain and the intermode kinetics with asymmetric intermode transitions.[144] This mechanism is formally identical to the one leading to equilibrium Bose–Einstein condensation of massive bosons. In experiments on coupled PhC nanolasers, the asymmetric intermode transitions resulted from stimulated scattering due to carrier population oscillations.[140] Cross-gain saturation is another mechanism to create pump-power-driven mode switching.[150] A further scheme to achieve a mode switching is based on injection seeding.[151,152]

4.4. Photon Number-Resolved Measurements

The individual photon-number distributions P_i and P_j for the strong and the weak mode have been measured in the few-photon regime using a superconducting transition edge sensor (TES).[153] Good agreement has been observed with a bimodal birth-death model introduced in ref. [138]. The most efficient way to solve the model are Monte Carlo simulations based on the Gillespie algorithm.[144]

More recently, a two-channel TES has been introduced that can simultaneously detect the photon number-resolved light emission of the two orthogonal modes.[146] An example of the resulting joint photon-number distribution P_{ij} is depicted in **Figure 6**. The presence of two well-separated peaks is the basis of the two-state model.[145] The peak with small j corresponds to state 1 (the strong mode is lasing and the weak mode is non-lasing), whereas the peak with small i corresponds to state 2. The faint "bridge" between these two peaks corresponds to transitions between state 1 and 2. If the transition time is sufficiently large, then the bimodal laser shows bistability and hysteresis.[139] The two peaks in P_{ij} carry over to a double-peak structure of the individual photon-number distributions P_i and P_j, demonstrating that both modes have a Poisson-like and a thermal-like contribution. The experimental results agree very well with an extended birth-death model including external degrees of freedom.[146]

4.5. Prospects

The bimodal high-β microcavity laser can be considered as an ideal superthermal light source as i) the coherence time is large (as opposed to a conventional thermal light source) and ii) the intensity fluctuations can be tuned simply by adjusting the injection current. The large intensity fluctuations and the corresponding high probability of photon pairs can be very useful for thermal ghost imaging,[154,155] photon-statistics excitation spectroscopy,[156] two-photon subwavelength lithography,[157] and two-photon luminescence microscopy.[158,159] Moreover, the superthermal light may improve the phase sensitivity in interferometry experiments,[160] help to detect subwavelength interference,[161] and improve the reconstruction of photon-number distributions.[162]

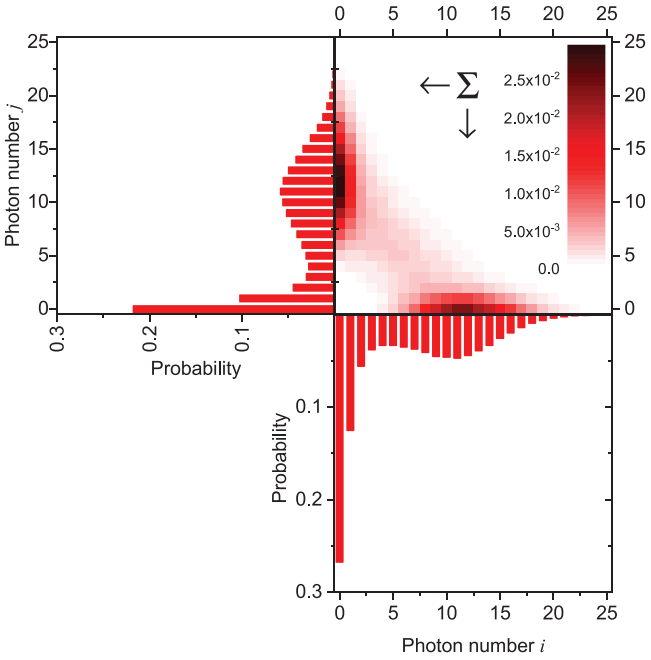

Figure 6. The joint photon-number distribution of a bimodal QD-micropillar laser far above threshold close to the switching point measured by a two-channel TES. Shown is also the individual photon-number distribution for the strong mode at the bottom and for the weak mode at the left axis calculated via a sum over the respective columns and rows. Adapted with permission.[146] Copyright 2021, American Physical Society.

Mode switching in bimodal microlasers might be exploited in the context of all-optical switching and low-power optical storage (see, e.g., refs. [151,152]).

Bimodal microlasers with time-delayed self-feedback provide a convenient platform to study nonlinear dynamics including chaos in the few-photon regime.[148,149] We expect that this merging of chaos and nanophotonics will result in a number of applications such as ultra-fast random bit generators, secure data communication with chaotic pulses, and novel schemes for information processing.

Micropillar cavities with elliptical cross section exhibit linearly polarized emission.[137] The coupling between carrier spin and light polarization can be exploited to generate fast polarization oscillations. This feature can render micropillar lasers excellent candidates for spin lasers, which promise low-energy ultrafast optical communication.[163]

5. Emerging Nanolaser Concepts

Going beyond the traditional scaling of microlasers toward nanolasers, very interesting concepts have emerged in recent years for new types of high-β lasers as well as lasers with unusual properties. These are based, among other things, on new

types of resonator geometries and new types of gain media, but also on unconventional physical principles. Against this background, the three following sections are dedicated to particularly promising new concepts.

5.1. Fano Lasers

The development of ultra-small in-plane lasers that emit light into on-chip waveguides is important for the development of a number of applications, like on-chip communication between the cores of a computer,[164] sensors, and quantum applications[165] (see Section 6.2). Recent years have seen impressive development of such lasers, in particular based on the PhC platform.[166,167] The development of electrical pumping schemes[168] and PhC buried heterostructure technology[169] are particularly important. The latter enables the integration of active and passive sections in the same waveguide layer. Evanescent coupling to silicon waveguides is also an important technology allowing to power silicon photonics circuits with ultrasmall lasers.[166]

Further progress in the field requires the development of lasers with many of the same features as found in macroscopic lasers, that is, high modulation bandwidth, low-noise, high quantum and wall-plug efficiency, robustness toward optical feedback, and different functionalities, such as generation of short optical pulses. The semiconductor Fano laser, theoretically suggested in ref. [171] and experimentally demonstrated in ref. [170], shows promise in meeting many of these requirements as well as displaying rich physics. This laser structure uses Fano interference effects to realize at least one of the mirrors. Fano interference is a general wave-interference phenomenon observed in many different physical systems, including quantum mechanics, optics, and plasmonics.[172,173] The Fano mirror in combination with nonlinearities gives the possibility to perform a range of optical signal processing functionalities, including wavelength conversion, pulse shortening, signal regeneration, and non-reciprocal diode characteristics.[174] In the context of lasers, the use of Fano interference allows for the implementation of a frequency-dependent mirror that only features a high reflectivity in a narrow frequency interval. This gives rise to fundamentally new laser dynamics, with several possible applications, such as strong frequency-selectivity, ultrahigh modulation bandwidth, pulse-generation, suppression of quantum noise, and increased resilience toward optical feedback.[175] The lasing mode in the Fano laser may be classified as a so-called bound-state-in-the-continuum,[176] relying on an intricate interference mechanism which produces a very sensitive mode-dependence on laser parameters[177] and imparts the laser with its characteristic features. The first experimental demonstration of a laser based on a bound-state-in-the-continuum was not achieved until recently.[178] The Fano laser represents another design for a bound-state-in-the-continuum and has the further advantage of in-plane emission.

Figure 7 shows a schematic of the Fano laser as it may be implemented in a PhC platform.[179,180] The figure shows a top view of a PhC membrane, where blue areas denote InP and white areas are airholes. Within the optical bandgap of the surrounding periodic PhC structure, in-plane confinement can be realized by defects, that is, missing or displaced airholes

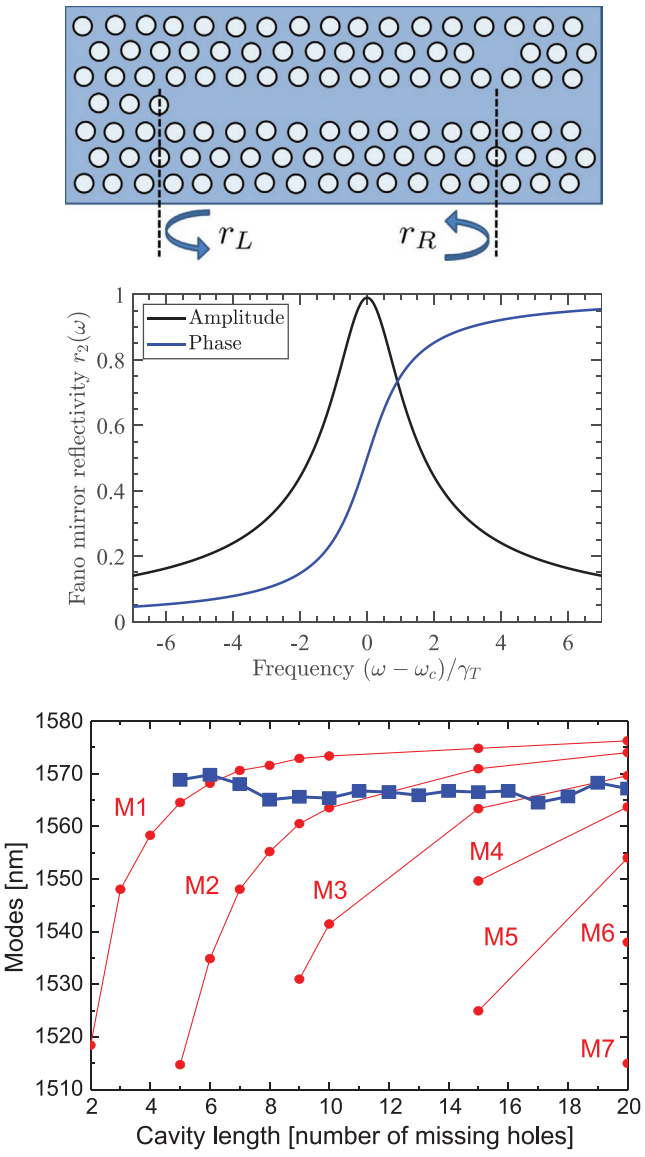

Figure 7. Upper: Schematic of a Fano laser. The left mirror is a conventional broadband photonic crystal mirror. The reflection of the right mirror is due to Fano interference between the field in the waveguide and the field in the side-coupled nanocavity, which here is implemented by omission of an air-hole. Middle: Frequency-dependent reflectivity of the Fano mirror. Lower: Comparison of measured mode resonances for Fano lasers (blue square markers) and line defect lasers (red circle markers) versus cavity length measured in number of "missing" holes between left and right mirror. Lower figure: Reproduced with permission.[170] Copyright 2017, Springer Nature.

making up waveguides (line defects) or localized cavities (point defects). Out-of plane confinement is realized by total internal reflection in the membrane, which has a height of the order of a few hundred nanometer. The left mirror of the laser cavity, with frequency-dependent reflectivity $r_L(\omega)$, is obtained by the conventional bandgap effect and has a relatively broad bandwidth.[181] The right mirror, with reflectivity $r_R(\omega)$, is instead due to Fano interference, realized by side-coupling a nanocavity to the waveguide.[182] Excited by light right-propagating in the

waveguide, the nanocavity's resonant field component destructively interferes with the waveguide's, thus preventing transmission and reflecting back the radiation in a bandwidth determined by the Q-factor.

The reflectivity of the Fano mirror, shown in Figure 7, can easily be calculated using coupled-mode-theory.[175,182] If Q_T denotes the total Q-factor of the nanocavity (including its coupling to the waveguide) and Q_i is the so-called intrinsic Q-factor (devoid of waveguide coupling, thus dominated by vertical diffraction losses), the maximum reflectivity of the Fano mirror is obtained at the resonance frequency ω_c and given by $|r_R(\omega_c)| = 1 - Q_T/Q_i$. Thus, achieving near-unity reflectivity for the Fano mirror only requires that the nanocavity's loss rate be dominated by coupling to the waveguide. The Fano mirror's 3-dB bandwidth is given by $2\gamma_T = \omega_c/Q_T$. Notice that the addition of an airhole in the waveguide below the nanocavity allows controlling the amplitude of the continuum path.[183] This turns the symmetric reflectivity profile seen in Figure 7 into an asymmetric one, useful for lowering switching energies.[174,183]

The lasing oscillation condition for the laser can be expressed as $r_L r_R \exp(ikL)$, where L is the distance between the left and right mirror and k is the complex wavenumber, the imaginary part of which accounts for the gain. The strong frequency dependence of the amplitude and phase of the Fano mirror reflectivity (see Figure 7) implies that the oscillation condition only is fulfilled when the laser oscillates very close to the resonance frequency of the nanocavity and simultaneously fulfills the phase condition at that frequency. This has the consequence that the laser only meets the oscillation condition for cavity lengths L that are within a few tens of nanometers from the optimum positions.[175]

In the experimental demonstration of the Fano laser,[170] the active gain material was composed of three layers of InAs QDs contained in the middle of the 250 nm thick InP membrane. The laser was optically pumped, at room temperature, by a continuous-wave laser beam focused to the laser cavity region between the two mirrors, while the nanocavity was unpumped. Figure 7 shows the measured lasing wavelength for Fano lasers with different lengths, obtained by changes of integer numbers of PhC periods. In all cases, the Fano laser operates on a single mode and oscillates close to the resonance of the nanocavity. In contrast, conventional line defect PhC lasers with two bandgap mirrors display a number of longitudinal optical modes, whose wavelengths change with cavity length, approaching the PhC bandedge where slow light effects lower the threshold gain.[184]

In the experiments,[170] the laser could operate both in a regime showing cw emission as well as in a regime where it emits a self-sustained train of short pulses at a repetition rate of a few gigahertz. Pulsing is explained as an example of passive Q-switching, promoted by un-pumped QDs in the nanocavity region of the Fano laser, which leads to a Fano mirror reflectivity that grows with laser intensity.[170,185] This is not unlike the use of semiconductor saturable mirrors to achieve pulse generation in VCSELs,[186] but in contrast to these, the Fano mirror is ultrasmall and monolithically integrated. The Fano laser dynamics can be modeled[171,185] by combining a general transmission line description of lasers[187] with dynamical coupled mode theory. Mathematically, the onset of self-pulsing can be understood as a generalized Hopf (Bautin) bifurcation[188] and the parameter region where it occurs has been identified.[185,188]

By using buried heterostructure technology[169] to limit the gain region to the waveguide region, the appearance of self-pulsing can be avoided and the nanocavity can instead be used to modulate the laser. It has been predicted[171,189] that the Fano laser can be directly modulated at frequencies up to several hundred gigahertz, without the usual limitation to a few tens of gigahertz imposed by the excitation of relaxation oscillations.[190] This modulation scheme uses the adiabatic wavelength conversion effect of an optical nanocavity,[180] where the wavelength of a field stored in a cavity may be changed dynamically by varying the refractive index of the cavity. By modulating the nanocavity of the Fano laser, preferentially through an applied electrical field, the laser signal thus becomes frequency modulated (FM-modulation). Since there is no, or little, variation of the laser intensity, the carrier density in the active laser waveguide is not modulated and accordingly the bandwidth is only limited by the ability to modulate the refractive index of the nanocavity. This is illustrated by the calculation in **Figure 8**,[175] which shows the amplitude of the FM modulation response and the corresponding modulation index. The experimental demonstration of this novel approach for laser modulation requires development of nanoelectrode technology, which is of general interest for further integrating optics and electronics.

It is well-known that semiconductor lasers can turn unstable due to even extremely small fractions of optical feedback. This is most important for practical applications, and usually demands the use of an optical isolator at the output of the laser. To date, however, there is no technology available for realizing integrated and ultra-small optical isolators, and therefore feedback-induced instabilities pose a challenge for on-chip micro- and nanolasers. One solution may be to use QD active material, so engineered as to reduce the linewidth enhancement factor α to

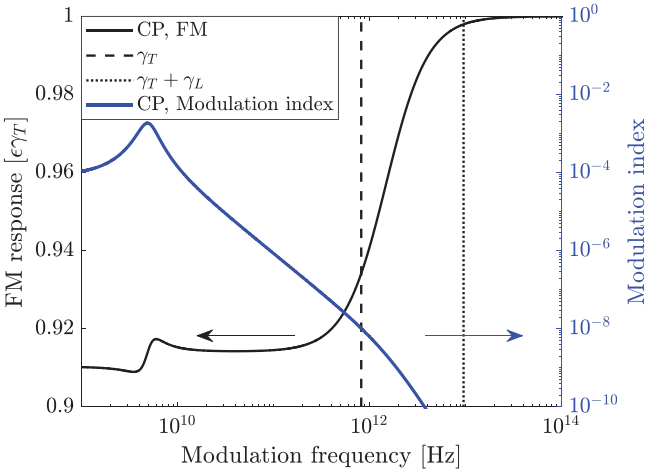

Figure 8. Frequency-modulation (FM) response (black) and modulation index (blue) for small-signal modulation of the the nanocavity resonance frequency. The modulated signal is extracted from a cross-port (CP) coupled to the nanocavity.[175] The dashed line indicates the characteristic frequency corresponding to the nanocavity decay rate, γ_T, and the dotted line is for the sum of the nanocavity decay rate and the inverse roundtrip time in the laser cavity, γ_L). Reproduced with permission.[175] Copyright 2019, IEEE.

a value close to zero, which strongly reduces the instability.[191] It was recently shown that the use of the Fano laser geometry provides another attractive solution for strongly improving the resilience of the laser towards optical feedback.[192] The feedback sensitivity was thus theoretically shown to be reduced by more than two orders of magnitude, an effect that can be traced back to an effective strong damping of relaxation oscillations due to temporal storage-effects of the nanocavity.[192]

5.2. Topological Microlasers

Topological insulators have attracted tremendous attention in the condensed matter community and beyond. Such a material is insulating in the bulk but exhibits conducting surface states that are protected by finite bulk band gaps and symmetries. In 2008 the concept was expanded into photonics,[193] see also.[194–197] The application to lasers was proposed and theoretically studied in 2013[198] and first realized experimentally in 2017.[199] Topological micro- and nanolasers promise to combine the robustness against disorder, defects, and sharp corners with single-mode lasing, an improved slope efficiency, a small footprint, and a low laser threshold.

5.2.1. 1D Systems

The original proposal of topological lasers[198] and its recent 1D realizations are based on the Su–Schrieffer–Hegger (SSH) chain. This tight-binding chain of dimers with alternating bonds between nearest-neighbor elements possesses two bands. A finite chain can host a midgap mode localized at the end of the chain or at domain walls. This mode, in contrast to conventional edge or defect modes, is not only protected by the finite bulk band gap that suppresses scattering into bulk modes, but also by a sublattice symmetry that ensures that the mode remains exactly in the middle of the gap.

A proper non-uniform distribution of gain and loss selects the edge mode,[198] as demonstrated in the microwave regime.[200] The first experiment on topological microlasers mimicked the SSH chain by a zigzag arrangement of coupled GaAlAs polariton micropillars with embedded GaAs QWs as gain material[201] (see **Figure 9**a). Further experiments were performed on coupled microrings containing InGaAsP QWs and supporting whispering-gallery modes (WGMs).[202,203] In ref. [203], the topological robustness was verified via structural deformations of the microring array. The same work also demonstrated large-area single-mode lasing resulting from the overlap of the edge mode with the inner part of the array. Topological lasing in exciton-polariton microcavity traps containing InGaAs QWs was realized in ref. [204].

The recent fabrication of topological nanolasers were based on high-β PhC structures.[205,206] Ref. [205] reported single-mode lasing in a GaAs PhC nanobeam containing InAs QDs, with small mode volume of $0.23(\lambda/n)^3$, an experimental (simulated) Q of ≈9600 (60000), and a spontaneous emission factor β of 0.03. In ref. [206], a PhC nanocavity with InAsP/InP QWs (Figure 9b) showed single-mode lasing with a simulated Q of ≈35000 and $\beta = 0.15$.

5.2.2. 2D Systems with Broken Time-Reversal Symmetry

2D topological photonic systems with broken time-reversal symmetry are the photonic analogues of the quantum Hall systems in condensed matter physics. The first experimental realization

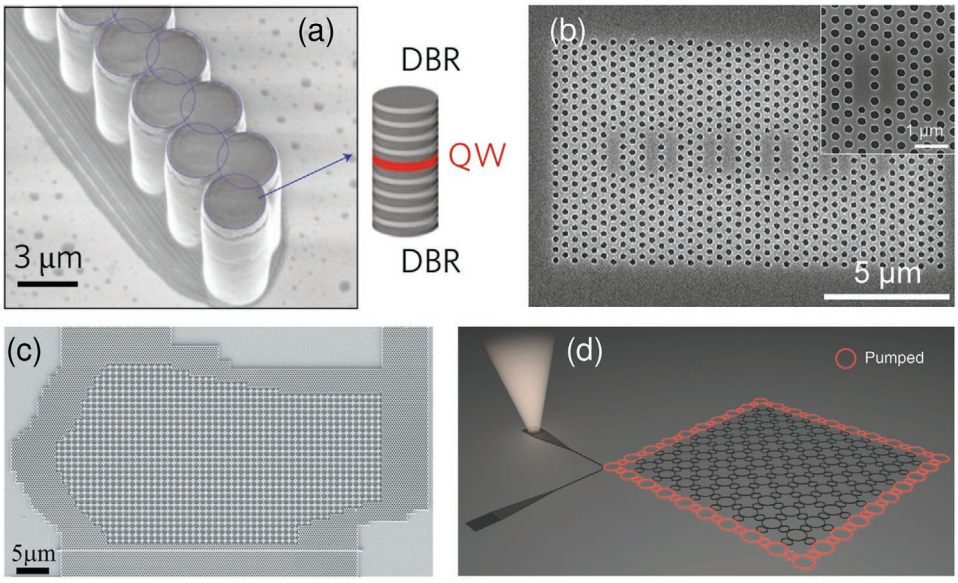

Figure 9. One- (top) and 2D (bottom) topological lasers. a) Scanning electron microscopy (SEM) image of a SSH chain of coupled micropillars. Reproduced with permission.[201] Copyright 2017, Springer Nature. b) SEM image of a PhC nanocavity. Reproduced with permission.[206] Copyright 2019, Springer Nature. c) SEM image of a cavity made of the USA-shaped boundary between two topologically inequivalent PhCs. The inner one has a star-shaped unit cell, the outer one a cylindrical air hole unit cell. Reproduced with permission.[199] Copyright 2019, Science. d) Schematic of an array of coupled microrings optically pumped along the perimeter to promote unidirectional edge-mode lasing. Reproduced with permission.[207] Copyright 2018, Science.

employed a PhC with embedded InGaAsP QWs[199] emitting at telecommunication wavelengths and at room temperature (see Figure 9c). A yttrium iron garnet (YIG) substrate was used to break time-reversal symmetry under a static external magnetic field. Even though the resulting topological band gap was narrow and the gain distribution was uniform, lasing on chiral modes has been observed. These tightly confined modes propagate unidirectionally along the edge being insensitive to its shape and to disorder. Such a unidirectional propagation allows an efficient phase locking and a reduction of spatial-hole burning.

5.2.3. 2D Systems with Time-Reversal Symmetry

2D topological photonic systems with time-reversal symmetry are the photonic analogues of quantum spin Hall systems. No external magnetic field is required here, but instead an internal symmetry, related to a pseudospin degree of freedom. The edge modes are helical, that is, they occur in counterpropagating pairs with equal frequency but opposite pseudospin. These modes are protected from backscattering into each other only if the above symmetry is preserved, that is, only for disorder of certain types.

The first demonstration used microring arrays on an InGaAsP QW platform,[207] with gain on the edges only (see Figure 9d). The pseudospin was here the orbital angular momentum in the rotational symmetric microrings. The nonlinear laser dynamics and the chosen excitation conditions selected one of the pseudospins resulting in unidirectional lasing. The pseudospin selection can be also biased by introducing asymmetric backscattering (see, e.g., ref. [208]) in the microrings.[207]

Most of the experiments on topological lasers have utilized optical pumping rather than electrical injection needed for applications. A recent experiment succeeded in electrically pumping THz quantum cascade lasers (GaAs/AlGaAs) using a valley PhC.[209] The latter is the photonic analogue of 2D gapped valleytronic materials. Negligible inter-valley scattering and therefore uncoupled valley pseudospins ensure that the helical edge modes are topologically protected. Numerical Q-factors of up to 10 000 were achieved. Another experiment demonstrated single-mode (simulated $Q \approx 20\,000$) topological lasing in a valley PhC with InGaAsP QWs at telecommunication wavelength under optical pumping.[210]

Higher-order topological states, such as corner modes, can provide sufficiently strong confinement needed for nanolasers. This was established for a GaAs PhC containing a single layer of InGaAs QDs.[211] A β-factor of 0.25 was measured, a mode volume of $0.61(\lambda/n)^3$ and a Q-factor up to 50 000 was calculated and an experimental Q-factor around 1700 was obtained. Room-temperature lasing of corner modes was demonstrated in a PhC slab accommodating InGaAsP QWs[212] with a simulated Q of ≈4000.

5.2.4. Prospects

The theoretical understanding of the coherence and the stability of topological lasers is still not well developed. While lasers with instantaneous gain saturation (class-A lasers) allow for dynamical stability,[213] there are indications that lasers with slow carrier dynamics (class-B lasers) can be dynamically unstable.[214] Recent theoretical studies showed that topological lasers in comparison to conventional laser arrays have a significantly improved temporal coherence in the presence of spatial disorder,[215] while in its absence, the temporal coherence is slightly below the conventional case, but the second-order photon autocorrelation function is still close to unity.[216] The latter was experimentally verified in refs. [204,217].

Even though large-area single-mode lasing is realized in topological lasers,[203] in most cases, the edge modes are exponentially localized in a few cavities of the array. There are a number of exciting new ideas to cure this problem, such as topological bulk lasing using an artificial imaginary gauge field[218,219] and frequency-selective band-inversion-induced reflection,[220] as well as exploiting synthetic dimensions.[221]

Further fascinating developments are the generation and multiplexing of light beams carrying orbital angular momentum,[217] and the in situ control of topological modes by non-Hermiticity, that is, gain and loss,[222] which for example, allows for the flexible reconfiguration of topological edge modes.[223] It can be anticipated that the rapidly advancing field of topological lasers hold further great opportunities for basic research and applications.

5.3. Nanolasers Based on 2D Quantum Materials

2D materials have emerged as a new class of crystalline gain media, following the discovery in 2010 that transition metal dichalcogenides (TMDs) become direct band-gap semiconductors in the monolayer limit.[224,225] The reduced dimensionality leads to reduced screening, large exciton binding energies, and strong optical transition dipole moment. Each monolayer is only about 0.7 nm thick but can absorb a few to a few tens of percent of light on a single pass, which suggests the potential of achieving high gain with a small number of injected carriers. Due to the absence of dangling bonds at the surface and weak inter-molecular layer van der Waals binding, 2D heterostructures can be crafted layer by layer, and integrated with different substrate without requiring lattice matching.[226] Thereby, new systems may be created where the media, the cavity modes, or both possess unusual properties, providing opportunities for new types of high-β factor nanolaser.

Taking advantage of the flexibility in integration, lasers have been built with monolayer TMDs directly placed on a variety of cavity architectures, including 2D PhC[227] and 1D nanobeam[228] cavities, micro-disks with WGMs,[229] and plasmonic nanoresonator arrays.[230] Lasing was identified by a super-linear increase in the emission intensity of the resonant mode as a function of the excitation intensity. These systems showed relatively low photon fluxes, large background from spontaneous emission, and a small linewidth reduction at the threshold. These properties have led to some skepticism of the nature of the observed super-linear power dependence.[231] On the other hand, these systems have similar configurations as those of QD lasers made of conventional materials. An interesting question is whether carrier localization has played an important role in these systems.

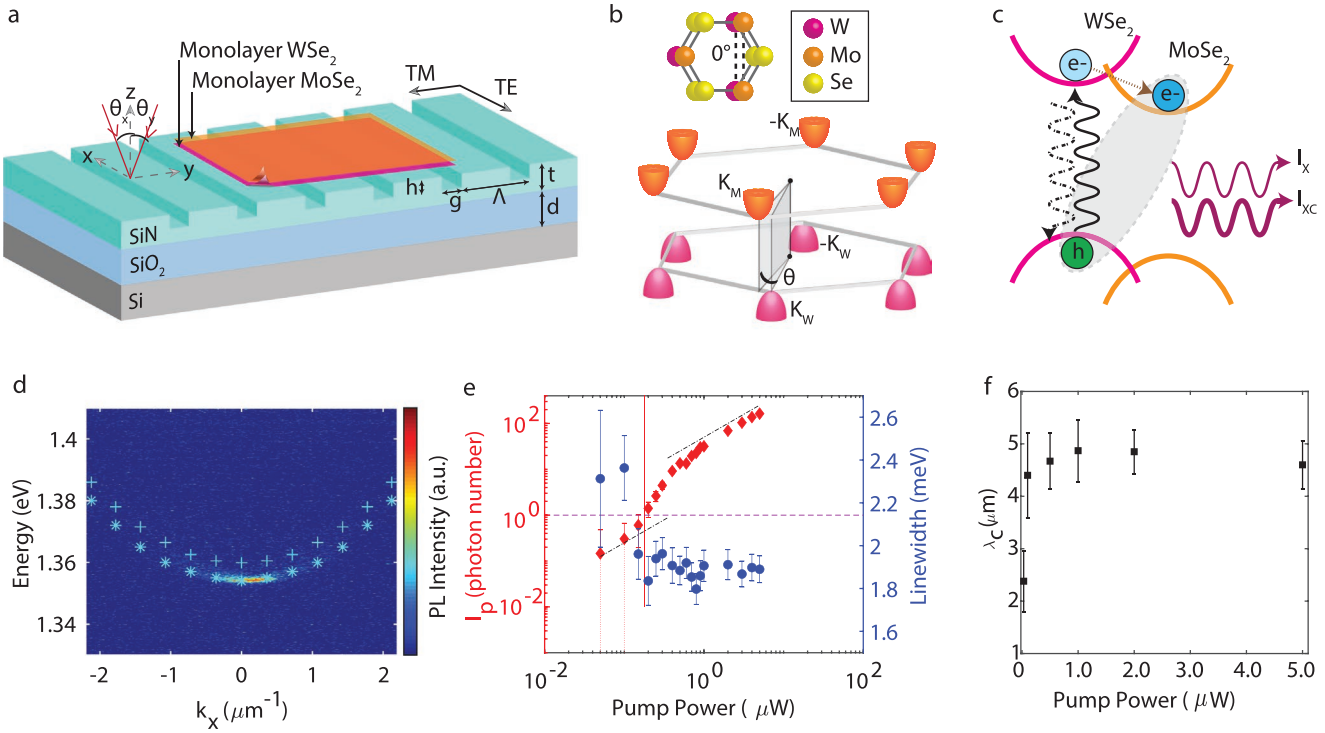

Figure 10. a) Schematic of the laser device consisting of a hetero-bilayer on a grating cavity. The TE-polarized guided wave resonance of the grating is near the interlayer exciton resonance of the hetero-bilayer. b) Illustration of the rotationally aligned hetero-bilayer with twist angle $\theta = 0°$ (left), and the corresponding band structure with extrema at the K-valleys (right). Depending on the twist angle θ, the hetero-bilayer has a direct or indirect bandgap. c) Band alignment and carrier dynamics of the hetero-bilayer. d) Angle-resolved spectra of the TE emission above lasing threshold, with overlaid simulated dispersions of the empty cavity (crosses) and cavity with bilayer (stars). e) The intensity (red) and linewidth (blue) of the TE emission from the hetero-bilayer versus input pump power. The emission intensity is integrated over $|k_x| < 0.7\ \mu m^{-1}$ and $|k_y| < 0.13\ \mu m^{-1}$. The dot-dashed line indicates a linear line, the vertical red line marks P_{th}, and the horizontal purple line indicates $I_p = 1$. f) The coherence length λ_c of the emission versus the pump power. Reproduced with permission.[232] Copyright 2019, Springer Nature.

While a monolayer forms the thinnest gain medium, it is insensitive to vertical electrical field and cannot form a vertical p-n junction. Each material typically has a preferred doping type, so it is often difficult to create high-quality lateral p- and n-contacts on the same monolayer. These difficulties can be circumvented using heterostructures. The simplest type of 2D heterostructures are formed by stacking two monolayers together. Laser emission, largely free from background spontaneous emission, was observed in a $MoSe_2/WSe_2$ hetero-bilayer placed directly on a 1D grating with guided-wave resonances[232] (**Figure 10**). The $MoSe_2/WSe_2$ hetero-bilayer has type-II band alignment. When the twist angle θ between the monolayer crystal orientations is close to the commensurate angles of 0° or 60°, a direct bandgap is formed. Carriers can be injected through the intralayer exciton resonance, followed by ultrafast charge transfer to the lower energy conduction band, while carrier losses due to radiative emission is suppressed. This allows efficient carrier build-up and population inversion. The 1D grating supports a spatially extended mode that couples to the full area of the 2D heterostructure. Therefore lasing leads to narrowing of the emission in the Fourier space near zero in-plane wavenumber, in addition to a super-linear increase of the emission intensity and linewidth reduction. A sharp increase in spatial coherence length above threshold pump power was observed, showing the formation of extended spatial coherence, supported by a 2D gain medium.

In the same type of hetero-bilayer, 1D and 2D moiré lattices have been reported.[233–236] It is therefore intriguing to ask whether a moiré lattice existed and played a key role in the hetero-bilayer laser. It is also important to understand the interplay between energy relaxation and radiative decay of the intra- and inter-layer transitions. A promising system for these studies is the $MoSe_2/WS_2$ hetero-bilayers. In $MoSe_2/WS_2$ hetero-bilayers, moiré lattices have been shown to form over a wide range of twist angles,[237,238] and the oscillator strength of the resulting moiré excitons are tunable via the twist angle.[238] Recent work shows that each moiré cell functions as a zero-dimensional QD with fully localized excitons of discrete energy levels.[239] The size of the moiré cell, corresponding to the period of the moiré lattice, is typically a few to a few tens of nanometers, similar to typical QDs. Compared to self-assembled QDs, such moiré "dots" are densely packed and do not have intrinsic structural or compositional inhomogeneities. As a result, the moiré-dot array can collectively couple with a cavity field, with a total oscillator strength comparable to that of a QW.[239] Therefore, the 2D moiré system may offer a new types of ensemble QD medium, which may be integrated with high-β factor nano-cavities developed for QD(s) as discussed in previous sections to enable high-*beta* factor lasers with high gain and efficiency.

While the science of 2D materials as a gain medium is still at infancy, future development of 2D material laser will also benefit greatly from the intense efforts on improving the quantum yield and fabrication technology of 2D material systems. Despite initial reports of less than 1% of quantum yield in TMD monolayers, recent work have shown proper passivation procedures may lead to near unity quantum yield in exfoliated monolayers[240] and over 60% in CVD-grown monolayers[241] at the room temperature. As technologies mature for scalable fabrication of 2D material heterostructures with high quantum yield, 2D material lasers may allow energy efficient, electrically injected, room temperature semiconductor nanolasers that are easily integrable with existing silicon-based photonics.

6. Applications of High-β Micro- and Nanolasers

In addition to their fundamental interest, high-β micro- and nanolasers hold great promise for applications thanks to their small component size and reduced threshold power. In addition, their tight mode confinement potentially enables the design of properties optimally tailored to specific applications. Three such areas are discussed here, as examples.

6.1. On-Chip Interconnects

It is well-known that photonics is a key enabling technology for the internet. Were it not for low-loss high-speed transmission of data in optical fibers as well as the efficient conversion between electrical and optical signals using semiconductor lasers and photodetectors, we would not have developed the information society and the global interconnectivity to nearly the level we are at today. Photonics is also being used for data communications inside data centers and there is increasing motivation for using optics even inside computer chips. Today, most of the energy dissipated inside computers is used to communicate rather than for logical operations.[164] Not only does this represent a significant fraction of global energy consumption, the generated heat limits the processor speed itself. The obvious solution is the of use optical interconnects, in the form of waveguides connecting different parts of the processor architecture. The advantages of using optics for interconnects are summarized in the following four points formulated by Miller:[164] 1) it can reduce interconnect energy by eliminating the charging of electrical lines; 2) it can send information over large distances at high rates without additional loss or distortion; 3) it can allow very high densities of high-bandwidth connections; 4) it can offer very precise timing and retiming of signals.

In order to benefit from the replacement of an electrical wire with an optical waveguide interconnect, the required energy per bit may have to be as low as a few tens of attojoules,[164] depending on the architecture. This condition puts stricts demands on the conversion efficiency from electronic to photonic bits (the laser) and vice versa (the photodetector). Furthermore, for such low-energy bits, shot noise becomes important and leads to bit-errors. Figure 11, following ref. [242] shows the calculated Bit-Error-Ratio (BER) versus number of photons in the bit for different noise distributions. As discussed earlier in this article (see Sections 2 and 3), a laser operating above threshold has Poissonian photon number statistics and the purple markers in Figure 11 show that in order to reach a BER of 10^{-20}, about 300 photons per bit are needed on average, corresponding to a bit energy of about 40 aJ at a wavelength of 1.55 μm. Notice that the requirement on the BER is much more stringent for communications between the cores of a computer than for normal internet traffic, where a BER of 10^{-9} often is considered "error-free" and where advanced error-correcting schemes may be employed.

This energy can be significantly reduced if one employs intensity-squeezed signals with sub-Poissonian statistics.[243] For a device generating a pure photon number state in the considered bit slot, no errors due to shot noise would be encountered if the effective loss of the link, including generation and detection efficiencies, were zero. It has been known since the work of Yamamoto et al. [244,245] that the output intensity noise of lasers can be reduced below the standard quantum limit by driving the laser with a so-called "quiet" electron stream. The combined effect of the degree of laser noise squeezing and the loss of the link can be described by a so-called Fano factor F, with $F = 1$ corresponding to Poisson statistics and $F = 0$ to a pure number state at the output of the link.[243] The corresponding effective efficiency in converting from the quiet electron stream to the photon stream is given by $\eta = 1 - F$. **Figure 11** shows the calculated BER for different values of η,[242] showing the large potential reduction of required photon number by using squeezed light.

The squeezing achieved in semiconductor lasers and LEDs[246–249] is limited by a number of factors, including side modes, intrinsic losses in the laser cavity,[250] and current leakage,[251] and the squeezing demonstrated so far has been limited to relatively small bandwidths that are typically insufficient for transmission of data. These limitations may to a large degree be overcome if the fundamental light–matter coupling in the device can be significantly enhanced. Recent designs[252–254] for achieving deep subwavelength confinement in an optical semiconductor cavity may provide a new approach for realizing such devices. Thus, while the Purcell factor in the conventional "good cavity limit," where the cavity bandwidth is

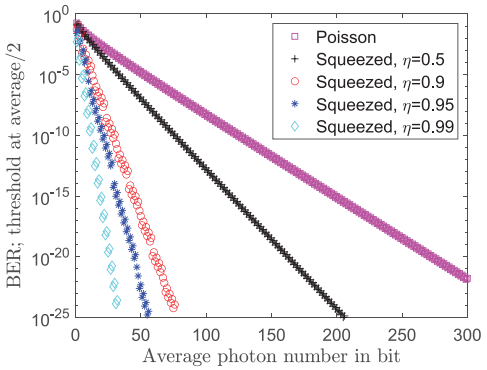

Figure 11. Bit-error-ratio (BER) versus average bit photon number for different noise distributions. The parameter η is related to the Fano factor by $F = 1 - \eta$, and is a measure of how well a quiet electrical pump current at the input is converted to a quiet photon stream at the output within the considered signal bandwidth.

smaller than the homogeneous emitter broadening, does not depend on the *Q*-factor, but it does depend on the inverse of the effective mode volume.[100,255] It was recently shown that by employing such a design for "extreme dielectric confinement," it should be feasible to realize a nanoLED featuring a high degree of squeezing in a large bandwidth.[242] The experimental realization of such novel deep-subwavelength laser cavities, without resorting to metal cavities and the strong losses that they bring,[256] is an important future challenge.

6.2. Quantum Nanophotonics

A second very interesting and suitable application scenario for high-β lasers is their use in the field of quantum nanophotonics. Here, these devices can act as coherent light sources for the resonant excitation of quantum emitters in order to generate single photons with high indistinguishability (in principle) on demand. Corresponding sources of indistinguishable photons are basic building blocks in photonic quantum technology. For instance, indistinguishable photons are required in long-distance quantum communication, which is based on the entanglement distribution via Bell state measurements.[257] Furthermore, indistinguishable photons are of high relevance as information carriers for boson sampling in the field of photonic quantum computing.[258,259]

In this context, it is important to mention that quantum emitters such as QDs can in principle be excited in pin-diode structures by electrical charge carrier injection to emit individual photons. However, the large number of free charge carriers in this intrinsically non-resonant type of excitation limits the indistinguishability of generated photons to values well below 50% even in state-of-the-art electrically driven single-photon sources.[260] Higher photon indistinguishability can be achieved by means of resonant excitation schemes, as has been shown many times in experiments in conventional laboratory setups under optical excitation with bulky (and expensive) commercial lasers. Particularly interesting is the strictly resonant excitation directly into the s-shell of the relevant QD, through which values of photon indistinguishability of over 99% were achieved.[261,262]

It is therefore extremely attractive to use monolithically integrated microlasers for the resonant optical excitation of quantum emitters. In this concept, compact sources of indistinguishable photons can be realized in a scalable way, for example, to provide modular quantum light sources in quantum communication and photonic state generators in photonic quantum computing.

The first application of a high-β laser in quantum nanophotonics was reported by Kreinberg et al.[263]. The aim of the work was to show that an electrically operated QD micropillar can be used for pulsed, strictly resonant excitation of a QD. This is a first step toward compact on-demand sources indistinguishable from the above concept. Its implementation is very challenging and places high demands on the optical quality of the microlaser. In fact, the laser must have an emission linewidth well below the homogeneous linewidth of the QD (typically 1 GHz), emit light pulses with a width well below the spontaneous life of the QD (typically 1 ns in a homogeneous medium and reduced to 100–200 ps for usual Purcell factors of 5–10 in micropillar systems[265]), and has to deliver a sufficiently high emission power to saturate the QD (typically 1 μW). Furthermore, the microlaser must be able to be sensitively brought into spectral resonance with the QD.

In the corresponding experiment, an electrically operated QD-micropillar laser in one cryostat was used to excite a single QD in a second cryostat via single-mode fiber coupling. The emission properties of the laser are presented in **Figure 12**. The single-mode device emits at around 919 nm and its

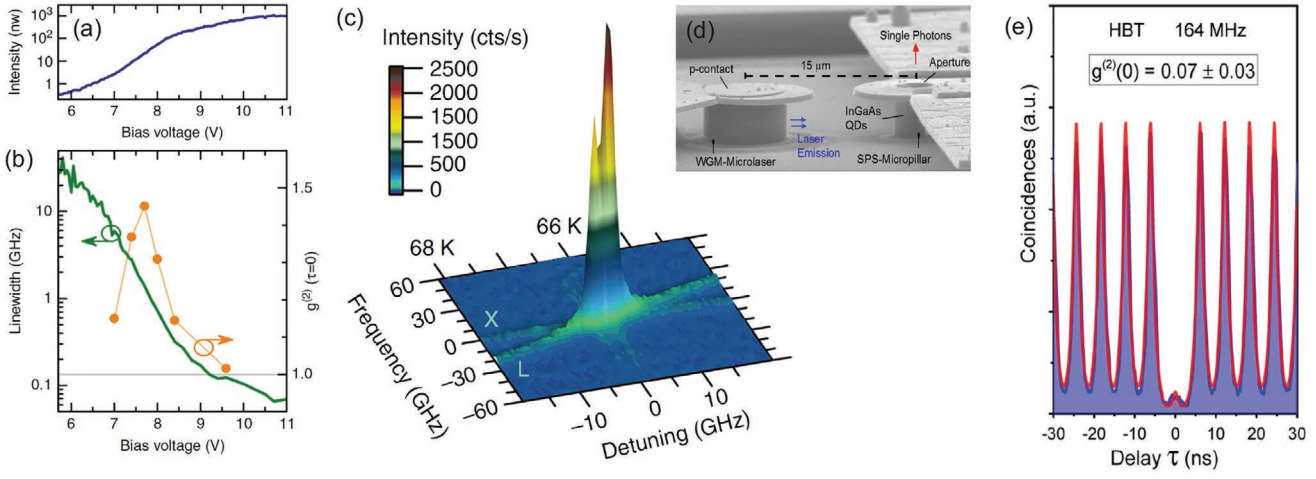

Figure 12. Application of an electrically driven QD-micropillar laser in quantum nanophotonics. a) Input–output characteristics of the monomode laser delivering up to 1 μW at 919 nm. b) Emission linewidth and equal-time second-order photon autocorrelation function as function of applied bias voltage. Laser emission with a linewidth as low as 50 MHz and is evidenced by the pronounced bias voltage dependent linewidth narrowing and the transition of $g^{(2)}(0)$ toward unity at high excitation strength. c) Resonance fluorescence intensity map indicating spectral resonance between the microlaser (L) and the QD s-shell (X) at a laser temperature of 66 K. d) SEM image of an integrated WGM-microlaser–SPS-micropillar configuration. e) Corresponding second-order photon autocorrelation function demonstrating triggered single-photon of the SPS-micropillar excited by the on-chip integrated WGM microlaser. a–c) Adapted with permission.[263] Copyright 2018, Springer Nature. d,e) Adapted with permission.[264] Copyright 2017, American Chemical Society.

input–output characteristic shows the typical s-shaped behavior of a high-β emitter and an output power up to 1 µW (panel (a)). Furthermore, in panel (b), a clear excitation-strength dependent decrease in the emission linewidth down to around 50 MHz can be observed. These features indicate lasing behavior with a threshold in the range of 7–8 volts bias voltage which is confirmed by measurements on the photon statistics with a characteristic maximum of (the convoluted) $g^{(2)}(0)$ dependence at threshold.[58,59]

These emission properties make the high-β microlaser a very attractive candidate for resonant excitation of a quantum emitter in quantum nanophotonics. In particular, the output power and the emission linewidth are in the necessary range for strict resonant excitation of a QD in order to observe resonance fluorescence and to generate individual photons with excellent quantum properties. In fact, in ref. [263], it was possible for the first time to use a high-β microlaser as coherent excitation source for a quantum optical experiment. As shown in Figure 12c, the laser was used to excite a QD (in the second cryostat) into its s-shell and thus to generate resonance fluorescence. The temperature of the laser was varied in the range from 64 to 68 K for the necessary spectral fine tuning between microlaser and QD. In spectral resonance at about 66 K, there is a significant increase in intensity, with the double peak feature in resonance fluorescence being attributed to the fine structure splitting of the QD. In this microlaser-QD configuration, the emission of individual photons with $g^{(2)}(0) = 0.02$ and an indistinguishability of 0.57(9) was achieved under pulsed-resonant excitation. The indistinguishability was limited on the one hand by a comparatively large pulse length of 200 ps (compared to an ideal pulse length of about 10 ps[261]) but also by the non-ideal properties of the QD itself, and it is expected to reach significantly higher indistinguishability values by technological improvements in the future.

While the application discussed is to be understood as an experimentally very complex proof-of-principle demonstration, it is interesting to mention that the underlying approach has already been implemented in a fully integrated concept.[264,266,267] A corresponding device is presented in Figure 12d. The SEM image shows an electrically operated WGM microlaser, which excites a single QD in a micropillar 15 µm away acting as single-photon source (SPS). Interestingly, the fact that micropillar cavities can emit also via WGMs was first reported in ref. [268], and first laser emission of WGMs in micropillar cavities was demonstrated in ref. [269], both under optical pumping. In the SPS micropillar, the Purcell effect is used to increase the photon extraction efficiency and the relevant QD-transition can be tuned in spectral resonance with the fundamental resonator mode by the quantum confined Stark effect using the electrical contact of the SPS-micropillar. It is interesting to note that this contact has a local aperture to separate the individual photons emitted from the stray light of the microlaser. In this configuration, with a repetition frequency of 165 MHz, it was possible to generate single photons with a $g^{(2)}(0) = 0.07$ under wetting-layer excitation as shown in Figure 12e.[264] In the future, it will be interesting to further optimize the integrated approach for strict resonant excitation and also to develop a waveguide coupling for microlaser integration in integrated quantum photonic circuits.[165]

All in all, the results presented in this section show the great potential of high-β micro- and nanolasers in a targeted and suitable manner to find an attractive application in the field of quantum nanophotonics.

6.3. Neuromorphic Computing

Instead of improving established von-Neumann-type computer architectures, for example, by using optical interconnects as discussed earlier, a radically different approach is to use neural network approaches, where weighted interactions between nodes and processing or decision-making at nodes are interweaved. Such schemes may, for example, be particularly useful for applications such as real-time data handling, computer vision and natural-language processing. In particular, it appears that neuromorphic computing schemes[270] may be able to exploit some of the key characteristic features of photonics, leading to promises of increasing the computation speed by several orders of magnitude, while simultaneously achieving excellent energy efficiencies.

Neuromorphic computing or signal processing schemes are inspired by the way neurons are used for processing information in our brains and one of the key challenges for photonics implementations is to develop photonic structures that can play the equivalent role of neurons.[270] The artificial photonic neurons making up the networks consist of two essential building blocks, illustrated in **Figure 13**, that is, a linear weighting and integration operation, where inputs from other neurons are accumulated with certain weighting functions, as well as a non-linear activation function, which determines whether that particular neuron should "fire" and generate an optical pulse for further transmission and processing in the network. The latter is essentially a thresholding characteristic, with demands on the pulse generated at the output and the period between pulses. These devices must be ultra-compact, compatible with dense integration, energy-efficient and fast, thus providing a very challenging overall task.[271]

There have been a number of suggestions for realizing the nonlinear activation function, which is key to the photonic neuron, including use of electro-absorption modulators,[272] micro-ring modulators,[273] as well as all-optical realizations like photonic reservoir computing.[274,275] A promising opportunity

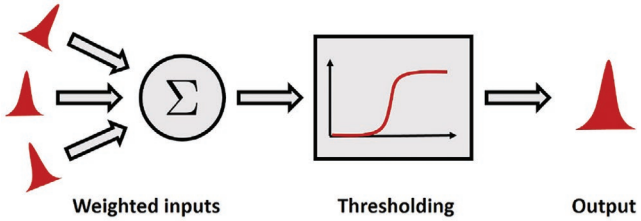

Figure 13. Schematic illustration of functionality needed in an artificial neuron-node in a neuromorphic computing scheme. Inputs from various nodes are weighted, summed, and sent as input to a thresholding device, where a nonlinear activation function decides whether the neuron should "fire" and generate an output pulse. Excitable semiconductor nanolasers may serve as the nonlinear element in such photonic neurons. The figure was inspired by ref. [270].

is to use excitable semiconductor lasers, which are reviewed in ref. [270]. The development of nanolasers for these functionalities are particularly attractive, given the need to integrate many nodes and the low energy available for each of those nodes. As an example, it has been theoretically shown that a semiconductor Fano laser (see Section 5.1) features intrinsic excitability and can be operated to give such a nonlinear thresholding functionality.[276] In this scheme, the nanocavity resonance is detuned from its optimal position such that the laser is operating in a below-threshold off-state. An optical pulse, representing the weighted input of other "spiking neurons", excites the nanocavity, and if the power is above the threshold level, the laser releases a new spike. The Fano laser features low threshold energy, gigahertz repetition rates, and orders of magnitude suppression between the on- and off-states.[276]

A related processing scheme is that of reservoir computing, where the network of interacting nodes is treated as a "black box", that is, the reservoir.[277] The training of the network is instead performed at the output to map many examples of inputs to desired outputs by invoking the right combination of reservoir states. The reservoir has to be "dynamic enough"[278] to sustain the desired processing complexity, but one has to avoid instabilities. Reservoir computing has been experimentally demonstrated on a silicon photonics chip, where the network itself is linear and the nonlinearity is implemented in the readout layer.[278]

A network of mutually coupled lasers appear as a particularly attractive way of implementing reservoir computing. This can for instance be achieved by optically coupling an array of VCSELS though an external diffractive element and using a spatial modulator for controlling individual coupling strengths.[275] The use of relatively large VCSELs as the individual elements of the array, however, imposes limitations on the reservoir dimension that can be achieved. Another approach is to use a dense array of energy efficient high-β micropillars.[279] Since the coupling relies on mutual injection locking between the lasers, the approach demands a high spectral homogeneity between the micropillar lasers. Promising progress in this direction was recently achieved through the demonstration of an array of 8×8 microlasers with spectral inhomogeneity below 200 μeV. This was achieved through the development of a nanoprocessing platform allowing for individual adjustments of laser wavelengths, and with the potential to be scaled to the coupling of hundreds of microlasers.

7. Conclusion

In summary, high-β micro- and nanolasers are innovative nanophotonic components with interesting physical properties and enormous application potential. Their development in the last two decades has benefited greatly from advances in modern nanotechnology, so that it was possible, for example, to reach the limiting case of thresholdless lasing. Furthermore, as we presented in this progress report, these miniaturized lasers provide a fertile basis for innovative ideas in order to explore new functional principles, based for instance on Fano resonators, topological effects, and 2D heterostructures, and to open up attractive areas of application in quantum photonics and neuromorphic computing. We hope that our article will not only provide an overview of the current status of micro- and nanolasers, but also stimulate further work and kick-start developments in order to tap the full potential of these exciting devices in an interdisciplinary and innovative research environment.

Acknowledgements

The authors acknowledge financial support by the German Research Foundation via projects Re2974/20-1, Re2974/21-1, Re2974/29-1, WI1986/11-1, by the Volkswagen Foundation via projects NeuroQNet1 and NeuroQNet2, and by the European Research Council under the European Union's Seventh Framework ERC Grant Agreement No. 615613 and No. 834410. Funding and support has also been provided by the Région PACA and Investments for the Future programme under the Université Côte d'Azur UCA-JEDI project managed by the ANR (ANR-15-IDEX-01) as well as the Danish National Research Foundation (DNRF147). The authors also acknowledge support by the United States Army Research Office Award W911NF-17-1-0312, Air Force Office of Scientific Research Award FA2386-18-1-4086, and the Humboldt Foundation's Friedrich Wilhelm Bessel Research Award. The authors would like to thank H. Schomerus for discussions.

Open access funding enabled and organized by Projekt DEAL.

Conflict of interest

The authors declare no conflict of interest.

Keywords

Fano lasers, high-β lasers, microlasers, nanolasers, neuromorphic computing, quantum nanophotonics, thresholdless lasing

Received: February 26, 2021
Revised: May 21, 2021
Published online: June 23, 2021

[1] W. W. Chow, S. Reitzenstein, *Appl. Phys. Rev.* **2018**, *5*, 041302.
[2] S. I. Azzam, A. V. Kildishev, R.-M. Ma, C.-Z. Ning, R. Oulton, V. M. Shalaev, M. I. Stockman, J.-L. Xu, X. Zhang, *Light: Sci. Appl.* **2020**, *9*, 20.
[3] M. Nomura, N. Kumagai, S. Iwamoto, Y. Ota, Y. Arakawa, *Opt. Express* **2009**, *17*, 15975.
[4] G. Björk, Y. Yamamoto, *IEEE J. Quantum Electron.* **1991**, *27*, 2386.
[5] M. Khajavikhan, A. Simic, M. Katz, J. H. Lee, B. Slutsky, A. Mizrahi, V. Lomakin, Y. Fainman, *Nature* **2012**, *482*, 204.
[6] H. Soda, K.-I. Iga, C. Kitahara, Y. Suematsu, *Jpn. J Appl. Phys.* **1979**, *18*, 2329.
[7] K. Iga, *IEEE J. Sel. Top. Quantum Electronics* **2000**, *6*, 1201.
[8] J. Jewell, S. McCall, Y.-H. Lee, A. Scherer, A. Gossard, J. English, *Appl. Phys. Lett.* **1989**, *54*, 1400.
[9] J. Jewell, K.-F. Huang, K. Tai, Y.-H. Lee, R. Fischer, S. McCall, A. Cho, *Appl. Phys. Lett.* **1989**, *55*, 424.
[10] D. Huffaker, J. Shin, D. Deppe, *Electron. Lett.* **1994**, *30*, 1946.
[11] G. Yang, M. MacDougal, P. Dapkus, *Electron. Lett.* **1995**, *31*, 886.
[12] M. H. MacDougal, P. D. Dapkus, V. Pudikov, H. Zhao, G. M. Yang, *IEEE Photonics Technol. Lett.* **1995**, *7*, 229.
[13] D. Huffaker, D. Deppe, *Appl. Phys. Lett.* **1997**, *71*, 1449.

[14] T. Baba, M. Fujita, A. Sakai, M. Kihara, R. Watanabe, *IEEE Photonics Technol. Lett.* **1997**, *9*, 878.
[15] A. E. Bond, P. D. Dapkus, J. D. O'brien, *IEEE Photonics Technol. Lett.* **1998**, *10*, 1362.
[16] J. L. Jewell, J. Harbison, A. Scherer, Y.-H. Lee, L. Florez, *IEEE J. Quantum Electron.* **1991**, *27*, 1332.
[17] D. Kleppner, *Phys. Rev. Lett.* **1981**, *47*, 233.
[18] P. W. Milonni, *Phys. Rev. A* **1982**, *25*, 1315.
[19] P. Goy, J. M. Raimond, M. Gross, S. Haroche, *Phys. Rev. Lett.* **1983**, *50*, 1903.
[20] R. G. Hulet, E. S. Hilfer, D. Kleppner, *Phys. Rev. Lett.* **1985**, *55*, 2137.
[21] D. Meschede, H. Walther, G. Müller, *Phys. Rev. Lett.* **1985**, *54*, 551.
[22] J. M. Gérard, B. Sermage, B. Gayral, B. Legrand, E. Costard, V. Thierry-Mieg, *Phys. Rev. Lett.* **1998**, *81*, 1110.
[23] J. McKeever, A. Boca, A. D. Boozer, J. R. Buck, H. J. Kimble, *Nature* **2003**, *425*, 268.
[24] F. De Martini, G. Innocenti, G. R. Jacobovitz, P. Mataloni, *Phys. Rev. Lett.* **1987**, *59*, 2955.
[25] F. D. Martini, G. R. Jacobovitz, *Phys. Rev. Lett.* **1988**, *60*, 1711.
[26] F. De Martini, M. Marrocco, P. Mataloni, L. Crescentini, R. Loudon, *Phys. Rev. A* **1991**, *43*, 2480.
[27] F. De Martini, F. Cairo, P. Mataloni, F. Verzegnassi, *Phys. Rev. A* **1992**, *46*, 4220.
[28] T. Baba, T. Hamano, F. Koyama, K. Iga, *IEEE J. Quantum Electron.* **1991**, *27*, 1347.
[29] Y. Yamamoto, S. Machida, G. Björk, *Phys. Rev. A* **1991**, *44*, 657.
[30] Y. Yamamoto, S. Machida, G. Björk, *Opt. Quantum Electron.* **1992**, *24*, S215.
[31] R. J. Horowicz, H. Heitmann, Y. Kadota, Y. Yamamoto, *Appl. Phys. Lett.* **1992**, *61*, 393.
[32] M. P. van Exter, A. K. J. Van Doorn, J. P. Woerdman, *IEEE J. Sel. Top. Quantum Electron.* **1995**, *1*, 601.
[33] E. M. Purcell, *Phys. Rev.* **1946**, *69*, 681.
[34] J.-M. Gérard, B. Gayral, *J. Lightwave Technol.* **1999**, *17*, 2089.
[35] H. W. Then, C. H. Wu, M. Feng, N. HolonyakJr., *Appl. Phys. Lett.* **2010**, *96*, 131107.
[36] M. P. van Exter, G. Nienhuis, J. P. Woerdman, *Phys. Rev. A* **1996**, *54*, 3553.
[37] P. Lalanne, *arXiv:2011.00218,* **2020**.
[38] F. T. Arecchi, R. Bonifacio, *IEEE J. Quantum Electron.* **1965**, *1*, 169.
[39] N. B. Abraham, L. M. Narducci, *Laser Physics and Laser Instabilities*, World Scientific, Singapore **1988**.
[40] G. J. de Valcárcel, E. Roldán, F. Prati, *Rev. Mex. Fis. E* **2006**, *52*, 198.
[41] E. del Valle, F. P. Laussy, *Phys. Rev. A* **2011**, *84*, 043816.
[42] S. Strauf, F. Jahnke, *Laser Photonics Rev.* **2011**, *5*, 607.
[43] A. Moelbjerg, P. Kaer, M. Lorke, B. Tromborg, J. Mork, *IEEE J. Quantum Electron.* **2013**, *49*, 945.
[44] L. A. Coldren, S. W. Corzine, *Diode Lasers and Photonic Integrated Circuits*, Wiley, New York **1995**.
[45] H. Yokoyama, S. D. Brorson, *J. Appl. Phys.* **1989**, *66*, 4801.
[46] H. Yokoyama, *Science* **1992**, *256*, 66.
[47] J. Gérard, O. Cabrol, B. Sermage, *Appl. Phys. Lett.* **1996**, *68*, 3123.
[48] T. Ide, T. Baba, J. Tatebayashi, S. Iwamoto, T. Nakaoka, Y. Arakawa, *Appl. Phys. Lett.* **2004**, *85*, 1326.
[49] J. B. Khurgin, M. A. Noginov, *Laser Photonics Rev.* **2021**, *15*, 2000250.
[50] P. R. Rice, H. J. Carmichael, *Phys. Rev. A* **1994**, *50*, 4318.
[51] T. Wang, D. Aktas, O. Alibart, É. Picholle, G. P. Puccioni, S. Tanzilli, G. L. Lippi, *Phys. Rev. A* **2020**, *101*, 063835.
[52] V. DeGiorgio, M. O. Scully, *Phys. Rev. A* **1970**, *2*, 1170.
[53] R. Graham, H. Haken, *Z. Phys.* **1970**, *237*, 31.
[54] S. Grossmann, P. H. Richter, *Z. Phys. A* **1971**, *242*, 458.
[55] V. Dohm, *Solid State Commun.* **1972**, *11*, 1273.
[56] G. Calo, A. D'Orazio, V. Petruzzelli, *J. Lightwave Technol.* **2012**, *30*, 944.
[57] M. R. Watts, J. Sun, C. DeRose, D. C. Trotter, R. W. Young, G. N. Nielson, *Opt. Lett.* **2013**, *38*, 733.
[58] S. Strauf, K. Hennessy, M. T. Rakher, Y.-S. Choi, A. Badolato, L. C. Andreani, E. L. Hu, P. M. Petroff, D. Bouwmeester, *Phys. Rev. Lett.* **2006**, *96*, 127404.
[59] S. M. Ulrich, C. Gies, S. Ates, J. Wiersig, S. Reitzenstein, C. Hofmann, A. Löffler, A. Forchel, F. Jahnke, P. Michler, *Phys. Rev. Lett.* **2007**, *98*, 043906.
[60] J. Wiersig, C. Gies, F. Jahnke, M. Aßmann, T. Berstermann, M. Bayer, C. Kistner, S. Reitzenstein, C. Schneider, S. Höfling, A. Forchel, C. Kruse, J. Kalden, D. Hommel, *Nature* **2009**, *460*, 245.
[61] W. E. Hayenga, H. Garcia-Gracia, H. Hodaei, C. Reimer, R. Morandotti, P. LiKamWa, M. Khajavikhan, *Optica* **2016**, *3*, 1187.
[62] S. H. Pan, Q. Gu, A. E. Amili, F. Vallini, Y. Fainman, *Optica* **2016**, *3*, 1260.
[63] S. Kreinberg, W. W. Chow, J. Wolters, C. Schneider, C. Gies, F. Jahnke, S. Höfling, M. Kamp, S. Reitzenstein, *Light: Sci. Appl.* **2017**, *6*, e17030.
[64] M. Takiguchi, A. Yokoo, K. Nozaki, M. D. Birowosuto, K. Tateno, G. Zhang, E. Kuramochi, A. Shinya, M. Notomi, *APL Photonics* **2017**, *2*, 046106.
[65] A. Kaganskiy, S. Kreinberg, X. Porte, S. Reitzenstein, *Optica* **2019**, *6*, 404.
[66] N. Takemura, M. Takiguchi, E. Kuramochi, A. Shinya, T. Sato, K. Takeda, S. Matsuo, M. Notomi, *Phys. Rev. A* **2019**, *99*, 053820.
[67] Vcsel-980manufacturer's specifications, https://www.thorlabs.com/drawings/f1dc547e03b5d3ab-8479AE6B-995E-2C5C-B7F89A4FB4C124F1/VCSEL-980-MFGSpec.pdf (accessed: January 2021).
[68] T. Wang, G. P. Puccioni, G. L. Lippi, *Sci. Rep.* **2015**, *5*, 15858.
[69] T. Wang, G. P. Puccioni, G. L. Lippi, in *Nanophotonics VI*, Proc. SPIE vol. 9884, International Society for Optics and Photonics, Bellingham, WA **2016**, p. 98840B.
[70] H. Yokoyama, *Science* **1992**, *256*, 66.
[71] K. D. Choquette, H. Q. Hou, K. L. Lear, H. C. Chui, K. M. Geib, A. Mar, B. E. Hammons, *Electron. Lett.* **1996**, *32*, 459.
[72] M. Sondermann, M. Weinkath, T. Ackemann, J. Mulet, S. Balle, *Phys. Rev. A* **2003**, *68*, 033822.
[73] R. E. Slusher, A. F. J. Levi, U. Mohideen, S. L. McCall, S. J. Pearton, R. A. Logan, *Appl. Phys. Lett.* **1993**, *63*, 1310.
[74] H. Cao, J. Y. Xu, W. H. Xiang, Y. Ma, S.-H. Chang, S. T. Ho, G. S. Solomon, *Appl. Phys. Lett.* **2000**, *76*, 3519.
[75] N. J. van Druten, Y. Lien, C. Serrat, S. S. R. Oemrawsingh, M. P. van Exter, J. P. Woerdman, *Phys. Rev. A* **2000**, *62*, 053808.
[76] Y. Lien, S. M. de Vries, N. J. van Druten, M. P. van Exter, J. P. Woerdman, *Phys. Rev. Lett.* **2001**, *86*, 2786.
[77] N. Takemura, M. Takiguchi, M. Notomi, *J. Opt. Soc. Am. B* **2021**, *38*, 699.
[78] J. P. Woerdman, M. P. van Exter, N. J. van Druten, in *Advances in Atomic, Molecular, and Optical Physics*, vol. 47, Elsevier, New York **2001**.
[79] T. Wang, G. P. Puccioni, G. L. Lippi, *J. Mod. Opt.* **2020**, *67*, 55.
[80] F. T. Arecchi, V. Degiorgio, *Phys. Rev. A* **1971**, *3*, 1108.
[81] S. Kreinberg, K. Laiho, F. Lohof, W. E. Hayenga, P. Holewa, C. Gies, M. Khajavikhan, S. Reitzenstein, *Laser Photonics Rev.* **2020**, *14*, 2000065.
[82] T. Wang, G. P. Puccioni, G. L. Lippi, *Ann. Phys.* **2018**, *530*, 1800086.
[83] T. Wang, H. Vergnet, G. P. Puccioni, G. L. Lippi, *Phys. Rev. A* **2017**, *96*, 013803.
[84] T. Wang, G. F. Wang, G. P. Puccioni, G. L. Lippi, *J. Opt. Soc. Am. B* **2019**, *36*, 799.
[85] T. Wang, X. Wang, Z. Deng, J. Sun, G. P. Puccioni, G. F. Wang, G. L. Lippi, *IEEE J. Sel. Top. Quantum Electron.* **2019**, *25*, 1700308.
[86] P. Wolf, P. Moser, G. Larisch, H. Li, J. Lott, D. Bimberg, *Electron. Lett.* **2013**, *49*, 666.

[87] H. Li, P. Wolf, P. Moser, G. Larisch, J. A. Lott, D. Bimberg, *IEEE J. Sel. Top. Quantum Electron.* **2015**, *21*, 405.
[88] D. M. Kuchta, A. V. Rylyakov, F. E. Doany, C. L. Schow, J. E. Proesel, C. W. Baks, P. Westbergh, J. S. Gustavsson, A. Larsson, *IEEE Photonics Technol. Lett.* **2015**, *27*, 577.
[89] C. Wagner, A. Dochhan, M. H. Eiselt, K. Grobe, M. Ortsiefer, C. Gréus, C. Neumeyr, S. Paul, J. Cesar, F. Küppers, et al., *IEEE Photonics Technol. Lett.* **2017**, *29*, 1475.
[90] D. A. Miller, *J. Lightwave Technol.* **2017**, *35*, 346.
[91] M. T. Hill, M. C. Gather, *Nat. Photonics* **2014**, *8*, 908.
[92] O. O. Moatlhodi, N. M. Ditshego, R. Samikannu, *J. Nano Res.* **2020**, *65*, 51.
[93] A. Einstein, *Phys. Z.* **1917**, *18*, 121.
[94] K. Roy-Choudhury, S. Haas, A. F. J. Levi, *Phys. Rev. Lett.* **2009**, *102*, 053902.
[95] K. Roy-Choudhury, A. F. J. Levi, *Phys. Rev. A* **2010**, *81*, 013827.
[96] A. Vallet, L. Chusseau, F. Philippe, A. Jean-Marie, *Phys. E* **2019**, *105*, 97.
[97] L. Chusseau, F. Philippe, F. Disanto, *Opt. Express* **2014**, *22*, 5312.
[98] A. Lebreton, I. Abram, N. Takemura, M. Kuwata-Gonokami, I. Robert-Philip, A. Beveratos, *New J. Phys.* **2013**, *15*, 033039.
[99] G. P. Puccioni, G. L. Lippi, *Opt. Express* **2015**, *23*, 2369.
[100] J. Mork, G. L. Lippi, *Appl. Phys. Lett.* **2018**, *112*, 141103.
[101] E. C. André, J. Mørk, M. Wubs, *Opt. Express* **2020**, *28*, 32632.
[102] G. L. Lippi, *Atoms* **2021**, *9*, 6.
[103] F. T. Arecchi, A. Berné, A. Sona, P. Burlamacchi, *IEEE J. Quantum Electron.* **1966**, *2*, 341.
[104] C. Gies, J. Wiersig, M. Lorke, F. Jahnke, *Phys. Rev. A* **2007**, *75*, 013803.
[105] W. W. Chow, F. Jahnke, *Prog. Quantum Electron.* **2013**, *37*, 109.
[106] M. Florian, C. Gies, F. Jahnke, H. A. M. Leymann, J. Wiersig, *Phys. Rev. B* **2013**, *87*, 165306.
[107] W. W. Chow, F. Jahnke, C. Gies, *Light: Sci. Appl.* **2014**, *3*, e201.
[108] H. A. M. Leymann, A. Foerster, J. Wiersig, *Phys. Rev. B* **2014**, *89*, 085308.
[109] M. A. Carroll, G. D'Alessandro, G. L. Lippi, G.-L. Oppo, F. Papoff, *Phys. Rev. Lett.* **2021**, *126*, 063902.
[110] C. Z. Ning, *IEEE J. Sel. Top. Quantum Electron* **2013**, *19*, 1503604.
[111] G. Björk, A. Karlsson, Y. Yamamoto, *Phys. Rev. A* **1994**, *50*, 1675.
[112] W. Barnes, G. Björk, J. Gérard, P. Jonsson, J. Wasey, P. Worthing, V. Zwiller, *Eur. Phys. J. D - At., Mol. Opt. Phys.* **2002**, *18*, 197.
[113] J. B. Khurgin, M. A. Noginov, *Laser Photonics Rev.* **2021**, *15*, 2000250.
[114] P. Michler, A. Kiraz, L. Zhang, C. Becher, E. Hu, A. Imamoglu, *Appl. Phys. Lett.* **2000**, *77*, 184.
[115] S. Reitzenstein, A. Bazhenov, A. Gorbunov, C. Hofmann, S. Münch, A. Löffler, M. Kamp, J. P. Reithmaier, V. D. Kulakovskii, A. Forchel, *Appl. Phys. Lett.* **2006**, *89*, 051107.
[116] H.-G. Park, J.-K. Hwang, J. Huh, H.-Y. Ryu, S.-H. Kim, J.-S. Kim, Y.-H. Lee, *IEEE J. Quantum Electron.* **2002**, *38*, 1353.
[117] Z. Xie, S. Götzinger, W. Fang, H. Cao, G. Solomon, *Phys. Rev. Lett.* **2007**, *98*, 117401.
[118] S. Reitzenstein, C. Böckler, A. Bazhenov, A. Gorbunov, A. Löffler, M. Kamp, V. D. Kulakovskii, A. Forchel, *Opt. Express* **2008**, *16*, 4848.
[119] M. Nomura, N. Kumagai, S. Iwamoto, Y. Ota, Y. Arakawa, *Nat. Phys.* **2010**, *6*, 279.
[120] C. Gies, F. Gericke, P. Gartner, S. Holzinger, C. Hopfmann, T. Heindel, J. Wolters, C. Schneider, M. Florian, F. Jahnke, S. Höfling, M. Kamp, S. Reitzenstein, *Phys. Rev. A* **2017**, *96*, 023806.
[121] M. T. Hill, M. Marell, E. S. P. Leong, B. Smalbrugge, Y. Zhu, M. Sun, P. J. van Veldhoven, E. J. Geluk, F. Karouta, Y.-S. Oei, R. Nötzel, C.-Z. Ning, M. K. Smit, *Opt. Express* **2009**, *17*, 11107.
[122] R. F. Oulton, V. J. Sorger, T. Zentgraf, R.-M. Ma, C. Gladden, L. Dai, G. Bartal, X. Zhang, *Nature* **2009**, *461*, 629.
[123] M. Takiguchi, H. Taniyama, H. Sumikura, M. D. Birowosuto, E. Kuramochi, A. Shinya, T. Sato, K. Takeda, S. Matsuo, M. Notomi, *Opt. Express* **2016**, *24*, 3441.
[124] Y. Ota, M. Kakuda, K. Watanabe, S. Iwamoto, Y. Arakawa, *Opt. Express* **2017**, *25*, 19981.
[125] I. Prieto, J. M. Llorens, L. E. Muñoz-Camúñez, A. G. Taboada, J. Canet-Ferrer, J. M. Ripalda, C. Robles, G. Muñoz-Matutano, J. P. Martínez-Pastor, P. A. Postigo, *Optica* **2015**, *2*, 66.
[126] S. T. Jagsch, N. V. Triviño, F. Lohof, G. Callsen, S. Kalinowski, I. M. Rousseau, R. Barzel, J.-F. Carlin, F. Jahnke, R. Butté, C. Gies, A. Hoffmann, N. Grandjean, S. Reitzenstein, *Nat. Commun.* **2018**, *9*, 564.
[127] A. L. Schawlow, C. H. Townes, *Phys. Rev.* **1958**, *112*, 1940.
[128] M. O. Scully, M. S. Zubairy, *Quantum Optics*, Cambridge University Press, Cambridge **1997**.
[129] F. Jahnke, C. Gies, M. Aßmann, M. Bayer, H. A. M. Leymann, A. Foerster, J. Wiersig, C. Schneider, M. Kamp, S. Höfling, *Nat. Commun.* **2016**, *7*, 11540.
[130] C. Redlich, B. Lingnau, S. Holzinger, E. Schlottmann, S. Kreinberg, C. Schneider, M. Kamp, S. Höfling, J. Wolters, S. Reitzenstein, K. Lüdge, *New J. Phys.* **2016**, *18*, 063011.
[131] M. Pelton, Y. Yamamoto, *Phys. Rev. A* **1999**, *59*, 2418.
[132] J.-M. Gérard, *Solid-State Cavity-Quantum Electrodynamics with Self-Assembled Quantum Dots*, Springer, Berlin, ISBN 978-3-540-39180-7 **2003**.
[133] F. Gericke, M. Segnon, M. von Helversen, C. Hopfmann, T. Heindel, C. Schneider, S. Höfling, M. Kamp, A. Musiał, X. Porte, C. Gies, S. Reitzenstein, *New J. Phys.* **2018**, *20*, 023036.
[134] W. Du, C. Li, J. Sun, H. Xu, P. Yu, A. Ren, J. Wu, Z. Wang, *Laser Photonics Rev.* **2020**, *14*, 2000271.
[135] S. Singh, L. Mandel, *Phys. Rev. A* **1979**, *20*, 2459.
[136] P. Lett, W. Christian, S. Singh, L. Mandel, *Phys. Rev. Lett.* **1981**, *47*, 1892.
[137] B. Gayral, J. M. Gérard, B. Legrand, E. Costard, V. Thierry-Mieg, *Appl. Phys. Lett.* **1998**, *72*, 1421.
[138] H. A. M. Leymann, C. Hopfmann, F. Albert, A. Foerster, M. Khanbekyan, C. Schneider, S. Höfling, A. Forchel, M. Kamp, J. Wiersig, S. Reitzenstein, *Phys. Rev. A* **2013**, *87*, 053819.
[139] S. Ishii, T. Baba, *Appl. Phys. Lett.* **2005**, *87*, 181102.
[140] M. Marconi, J. Javaloyes, F. Raineri, J. A. Levenson, A. M. Yacomotti, *Opt. Lett.* **2016**, *41*, 5628.
[141] F. Marconi, M.and Raineri, J. A. Levenson, A. M. Yacomotti, *Phys. Rev. Lett.* **2020**, *124*, 21360.
[142] M. Khanbekyan, H. A. M. Leymann, C. Hopfmann, A. Foerster, C. Schneider, S. Höfling, M. Kamp, J. Wiersig, S. Reitzenstein, *Phys. Rev. A* **2015**, *91*, 043840.
[143] P. Hamel, S. Haddadi, F. Raineri, P. Monnier, G. Beaudoin, I. Sagnes, A. Levenson, A. M. Yacomotti, *Nat. Photonics* **2015**, *9*, 311.
[144] H. A. M. Leymann, D. Vorberg, T. Lettau, C. Hopfmann, C. Schneider, M. Kamp, S. Höfling, R. Ketzmerick, J. Wiersig, S. Reitzenstein, A. Eckardt, *Phys. Rev. X* **2017**, *7*, 021045.
[145] T. Lettau, H. A. M. Leymann, B. Melcher, J. Wiersig, *Phys. Rev. A* **2018**, *97*, 053835.
[146] M. Schmidt, I. H. Grothe, S. Neumeier, L. Bremer, M. von Helversen, W. Zent, B. Melcher, J. Beyer, C. Schneider, S. Höfling, J. Wiersig, S. Reitzenstein, *Physical Review Research (in press)* **2021**.
[147] E. Schlottmann, D. Schicke, F. Krüger, B. Lingnau, C. Schneider, M. Kamp, S. Höfling, K. Lüdge, X. Porte, S. Reitzenstein, *Opt. Express* **2019**, *20*, 28816.
[148] F. Albert, C. Hopfmann, S. Reitzenstein, C. Schneider, S. Höfling, L. Worschech, M. Kamp, W. Kinzel, A. Forchel, I. Kanter, *Nat. Commun.* **2011**, *2*, 336.
[149] C. Hopfmann, F. Albert, C. Schneider, S. Höfling, M. Kamp, A. Forchel, I. Kanter, S. Reitzenstein, *New J. Phys.* **2013**, *15*, 025030.

[150] L. Ge, D. Liu, A. Cerjan, S. Rotter, H. Cao, S. G. Johnson, H. E. Türeci, A. D. Stone, *Opt. Express* **2016**, *24*, 41.
[151] M. T. Hill, H. J. S. Dorren, T. de Vries, X. J. M. Leijtens, J. H. den Besten, B. Smalbrugge, Y.-S. Oei, H. Binsma, G.-D. Khoe, M. K. Smit, *Nature* **2004**, *432*, 206.
[152] S. V. Zhukovsky, D. N. Chigrin, A. V. Lavrinenko, J. Kroha, *Phys. Rev. Lett.* **2007**, *99*, 073902.
[153] E. Schlottmann, M. von Helversen, H. A. M. Leymann, T. Lettau, F. Krüger, M. Schmidt, C. Schneider, M. Kamp, S. Höfling, J. Beyer, J. Wiersig, S. Reitzenstein, *Phys. Rev. Appl.* **2018**, *9*, 064030.
[154] R. S. Bennink, S. J. Bentley, R. W. Boyd, *Phys. Rev. Lett.* **2002**, *89*, 113601.
[155] A. Gatti, E. Brambilla, M. Bache, L. A. Lugiato, *Phys. Rev. Lett.* **2004**, *93*, 093602.
[156] T. Kazimierczuk, J. Schmutzler, M. Aßmann, C. Schneider, M. Kamp, S. Höfling, M. Bayer, *Phys. Rev. Lett.* **2015**, *115*, 027401.
[157] D.-Z. Cao, G.-J. Ge, K. Wang, *Appl. Phys. Lett.* **2010**, *97*, 051105.
[158] W. Denk, J. H. Strickler, W. W. Webb, *Science* **1990**, *248*, 73.
[159] A. Jechow, M. Seefeldt, H. Kurzke, A. Heuer, R. Menzel, *Nat. Photonics* **2013**, *7*, 973.
[160] S. M. H. Rafsanjani, M. Mirhosseini, O. S. M. na Loaiza, B. T. Gard, R. Birrittella, B. E. Koltenbah, C. G. Parazzoli, B. A. Capron, C. C. Gerry, J. P. Dowling, R. W. Boyd, *Optica* **2017**, *4*, 487.
[161] Y. Zhai, F. E. Becerra, J. Fan, A. Migdall, *Appl. Phys. Lett.* **2014**, *105*, 101104.
[162] G. Harder, D. Mogilevtsev, N. Korolkova, C. Silberhorn, *Phys. Rev. Lett.* **2014**, *113*, 070403.
[163] M. Lindemann, G. Xu, T. Pusch, R. Michalzik, M. R. Hofmann, I. Žutić, N. C. Gerhardt, *Nature* **2019**, *568*, 212.
[164] D. A. B. Miller, *J. Lightwave Technol.* **2017**, *35*, 346.
[165] S. Rodt, S. Reitzenstein, *APL Photon.* **2021**, *6*, 010901.
[166] G. Crosnier, D. Sanchez, S. Bouchoule, P. Monnier, G. Beaudoin, I. Sagnes, R. Raj, F. Raineri, *Nat. Photonics* **2017**, *11*, 297.
[167] S. Matsuo, T. Kakitsuka, *Adv. Opt. Photonics* **2018**, *10*, 567.
[168] H.-G. Park, S.-H. Kim, S.-H. Kwon, Y.-G. Ju, J.-K. Yang, J.-H. Baek, S.-B. Kim, Y.-H. Lee, *Science* **2004**, *305*, 1444.
[169] S. Matsuo, A. Shinya, T. Kakitsuka, K. Nozaki, T. Segawa, T. Sato, Y. Kawaguchi, M. Notomi, *Nat. Photonics* **2010**, *4*, 648.
[170] Y. Yu, W. Xue, E. Semenova, K. Yvind, J. Mork, *Nat. Photonics* **2017**, *11*, 81.
[171] J. Mork, Y. Chen, M. Heuck, *Phys. Rev. Lett.* **2014**, *113*, 163901.
[172] A. E. Miroshnichenko, S. Flach, Y. S. Kivshar, *Rev. Mod. Phys.* **2010**, *82*, 2257.
[173] M. F. Limonov, M. V. Rybin, A. N. Poddubny, Y. S. Kivshar, *Nat. Photonics* **2017**, *11*, 543.
[174] D. Bekele, Y. Yu, K. Yvind, J. Mork, *Laser Photonics Rev.* **2019**, *13*, 1900054.
[175] J. Mork, Y. Yu, T. S. Rasmussen, E. Semenova, K. Yvind, *IEEE J. Sel. Top. Quantum Electron.* **2019**, *25*, 8734739.
[176] C. W. Hsu, B. Zhen, A. D. Stone, J. D. Joannopoulos, M. Soljačić, *Nat. Rev. Mater.* **2016**, *1*, 16048.
[177] M. Rybin, Y. Kivshar, *Nature* **2017**, *541*, 164.
[178] A. Kodigala, T. Lepetit, Q. Gu, B. Bahari, Y. Fainman, B. Kanté, *Nature* **2017**, *541*, 196.
[179] S. Johnson, P. Villeneuve, S. Fan, J. Joannopoulos, *Phys. Rev. B* **2000**, *62*, 8212.
[180] M. Notomi, *Rep. Prog. Phys.* **2010**, *73*, 096501.
[181] P. Lalanne, C. Sauvan, J. P. Hugonin, *Laser Photon. Rev.* **2008**, *2*, 514.
[182] S. Fan, *Appl. Phys. Lett.* **2002**, *80*, 908.
[183] M. Heuck, P. T. Kristensen, Y. Elesin, J. Mork, *Opt. Lett.* **2013**, *38*, 2466.
[184] W. Xue, Y. Yu, L. Ottaviano, Y. Chen, E. Semenova, K. Yvind, J. Mork, *Phys. Rev. Lett.* **2016**, *116*, 063901.
[185] T. S. Rasmussen, Y. Yu, J. Mork, *Laser Photonics Rev.* **2017**, *11*, 1700089.
[186] U. Keller, K. Weingarten, *IEEE J. Sel. Top. Quantum Electron.* **1996**, *2*, 435.
[187] B. Tromborg, H. Olesen, X. Pan, S. Saito, *IEEE J. Quantum Electron.* **1987**, *QE-23*, 1875.
[188] P. M. Kaminski, S. Arslanagic, J. Mørk, J. Li, *Phys. Rev. A* **2019**, *100*, 053808.
[189] T. S. Rasmussen, Y. Yu, J. Mork, *Opt. Express* **2018**, *26*, 16365.
[190] L. A. Coldren, S. W. Corzine, M. L. Masanovic, *Diode Lasers and Photonic Integrated Circuits*, 2nd ed., Wiley, New York **2012**.
[191] H. Huang, J. Duan, D. Jung, A. Y. Liu, Z. Zhang, J. Norman, J. E. Bowers, F. Grillot, *J. Opt. Soc. Am. B* **2018**, *35*, 2780.
[192] T. S. Rasmussen, Y. Yu, J. Mork, *Phys. Rev. Lett.* **2019**, *123*, 233904.
[193] F. D. Haldane, S. Raghu, *Phys. Rev. Lett.* **2008**, *100*, 013904.
[194] M. Hafezi, E. A. Demler, M. D. Lukin, J. M. Taylor, *Nat. Phys.* **2011**, *7*, 907.
[195] L. Lu, J. D. Joannopoulos, Soljacić, *Nat. Photonics* **2014**, *8*, 821.
[196] T. Ozawa, H. M. Price, A. Amo, N. Goldman, M. Hafezi, L. Lu, M. C. Rechtsman, D. Schuster, J. Simon, O. Zilberberg, I. Carusotto, *Rev. Mod. Phys.* **2019**, *91*, 015006.
[197] D. Smirnova, D. Leykam, Y. Chong, Y. Kivshar, *Appl. Phys. Rev.* **2020**, *7*, 021306.
[198] H. Schomerus, *Opt. Lett.* **2013**, *38*, 1912.
[199] B. Bahari, A. Ndao, F. Vallini, A. E. Amili, Y. Fainman, B. Kanté, *Science* **2017**, *358*, 636.
[200] C. Poli, M. Bellec, U. Kuhl, F. Mortessagne, H. Schoermus, *Nat. Commun.* **2015**, *6*, 6710.
[201] P. St-Jean, V. Goblot, E. Galopin, A. Lemaítre, T. Ozawa, L. Le Gratiet, I. Sagnes, J. Bloch, A. Amo, *Nat. Photonics* **2017**, *11*, 651.
[202] M. Parto, S. Wittek, H. Hodaei, G. Harari, M. A. Brandres, J. Ren, M. C. Rechtsman, M. Segev, D. Christodoulides, M. Khajavikhan, *Phys. Rev. Lett.* **2018**, *120*, 113901.
[203] H. Zhao, P. Miao, M. H. Teimourpour, S. Malzard, R. El-Ganainy, H. Schomerus, L. Feng, *Nat. Commun.* **2018**, *9*, 981.
[204] T. H. Harder, M. Sun, O. A. Egorov, I. Vakulchyk, J. Beierlein, P. Gagel, M. Emmerling, C. Schneider, U. Peschel, I. G. Savenko, S. Klembt, S. Höfling, *arXiv:2005.14546* **2020**.
[205] Y. Ota, R. Katsumi, K. Watanabe, S. Iwamoto, Y. Arakawa, *Commun. Phys.* **2018**, *1*, 86.
[206] C. Han, M. Lee, S. Callard, C. Seassal, H. Jeon, *Light: Sci. Appl.* **2019**, *8*, 40.
[207] M. A. Brandres, S. Wittek, G. Harari, M. Parto, J. Ren, M. C. Rechtsman, M. Segev, D. Christodoulides, M. Khajavikhan, *Science* **2018**, *359*, 1231.
[208] J. Wiersig, in *Parity-Time Symmetry and Its Applications*, Springer, Singapore **2018**, pp. 155–184.
[209] Y. Zeng, U. Chattopadhyay, B. Zhu, B. Qiang, J. Li, Y. Jin, L. Li, A. G. Davis, E. H. Linfield, B. Zhang, Y. Chong, Q. J. Wang, *Nature* **2020**, *578*, 246.
[210] W. Noh, H. Nasari, H.-M. Kim, Q. Le-Van, Z. Jia, C.-H. Huang, B. Kanté, *Opt. Lett.* **2020**, *45*, 4108.
[211] W. Zhang, X. Xie, H. Hao, J. Dang, S. Xiao, S. Shi, H. Ni, Z. Niu, C. Wang, K. Jin, X. Zhang, X. Xu, *Light: Sci. Appl.* **2020**, *9*, 109.
[212] D. Smirnova, A. Tripathi, S. Kruk, M.-S. Hwang, H.-R. Kim, H.-G. Park, Y. Kivshar, *Light: Sci. Appl.* **2020**, *9*, 127.
[213] S. Malzard, H. Schomerus, *New J. Phys.* **2018**, *20*, 063044.
[214] S. Longhi, Y. Kominis, V. Kovanis, *Europhys. Lett.* **2018**, *122*, 14004.
[215] I. Amelio, I. Carusotto, *Phys. Rev. X* **2020**, *10*, 041060.
[216] P. Zapletal, B. Galilo, A. Nunnenkamp, *Optica* **2020**, *7*, 1045.
[217] B. Bahari, L.-Y. Hsu, H. Pan, D. Preece, A. Ndao, A. E. Amili, Y. Fainman, B. Kanté, in *Frontiers in Optics + Laser Science APS/DLS*, Optical Society of America, Washington, DC **2019** pp. LM3E.3–LM3E.3.

[218] S. Longhi, *Ann. Phys. (NY)* **2018**, *530*, 1800023.
[219] S. Wong, S. S. Oh, *arXiv:2012.09684*, **2020**.
[220] Z.-K. Shao, H.-Z. Chen, S. Wang, X.-R. Mao, Z.-Q. Yang, S.-L. Wang, X.-X. Wang, X. Hu, R.-M. Ma, *Nat. Nanotechnol.* **2020**, *15*, 67.
[221] Z. Yang, E. Lustig, H. G., Y. Plotnik, Y. Lumer, M. A. Brandes, M. Segev, *Phys. Rev. X* **2020**, *10*, 011059.
[222] K. Takata, M. Notomi, *Phys. Rev. Lett.* **2018**, *121*, 213902.
[223] H. Zhao, X. Qiao, T. Wu, B. Midya, S. Longhi, L. Feng, *Science* **2019**, *365*, 1163.
[224] A. Splendiani, L. Sun, Y. Zhang, T. Li, J. Kim, C.-Y. Chim, G. Galli, F. Wang, *Nano Lett.* **2010**, *10*, 1271.
[225] K. F. Mak, C. Lee, J. Hone, J. Shan, T. F. Heinz, *Phys. Rev. Lett.* **2010**, *105*, 136805.
[226] A. K. Geim, I. V. Grigorieva, *Nature* **2013**, *499*, 419.
[227] S. Wu, S. Buckley, J. R. Schaibley, L. Feng, J. Yan, D. G. Mandrus, F. Hatami, W. Yao, J. Vučković, A. Majumdar, X. Xu, *Nature* **2015**, *520*, 69.
[228] Y. Li, J. Zhang, D. Huang, H. Sun, F. Fan, J. Feng, Z. Wang, C. Z. Ning, *Nature Nanotechnol* **2017**.
[229] O. Salehzadeh, M. Djavid, N. H. Tran, I. Shih, Z. Mi, *Nano Lett.* **2015**, *15*, 5302.
[230] Y. Ye, Z. J. Wong, X. Lu, X. Ni, H. Zhu, X. Chen, Y. Wang, X. Zhang, *Nat. Photonics* **2015**, *9*, 733.
[231] L. Reeves, Y. Wang, T. F. Krauss, *Adv. Optical Mater.* **2018**, 1800272.
[232] E. Y. Paik, L. Zhang, G. W. Burg, R. Gogna, E. Tutuc, H. Deng, *Nature* **2019**, *576*, 80.
[233] K. Tran, G. Moody, F. Wu, X. Lu, J. Choi, K. Kim, A. Rai, D. A. Sanchez, J. Quan, A. Singh, J. Embley, A. Zepeda, M. Campbell, T. Autry, T. Taniguchi, K. Watanabe, N. Lu, S. K. Banerjee, K. L. Silverman, S. Kim, E. Tutuc, L. Yang, A. H. MacDonald, X. Li, *Nature* **2019**, *567*, 71.
[234] K. L. Seyler, P. Rivera, H. Yu, N. P. Wilson, E. L. Ray, D. G. Mandrus, J. Yan, W. Yao, X. Xu, *Nature* **2019**, *567*, 66.
[235] L. J. McGilly, A. Kerelsky, N. R. Finney, K. Shapovalov, E.-M. Shih, A. Ghiotto, Y. Zeng, S. L. Moore, W. Wu, Y. Bai, K. Watanabe, T. Taniguchi, M. Stengel, L. Zhou, J. Hone, X. Zhu, D. N. Basov, C. Dean, C. E. Dreyer, A. N. Pasupathy, *Nat. Nanotechnol.* **2020**, *15*, 580.
[236] Y. Bai, L. Zhou, J. Wang, W. Wu, L. J. McGilly, D. Halbertal, C. F. B. Lo, F. Liu, J. Ardelean, P. Rivera, N. R. Finney, X.-C. Yang, D. N. Basov, W. Yao, X. Xu, J. Hone, A. N. Pasupathy, X.-Y. Zhu, *Nat. Mater.* **2020**, *19*, 1068.
[237] E. M. Alexeev, D. A. Ruiz-Tijerina, M. Danovich, M. J. Hamer, D. J. Terry, P. K. Nayak, S. Ahn, S. Pak, J. Lee, J. I. Sohn, M. R. Molas, M. Koperski, K. Watanabe, T. Taniguchi, K. S. Novoselov, R. V. Gorbachev, H. S. Shin, V. I. Fal'ko, A. I. Tartakovskii, *Nature* **2019**, *567*, 81.
[238] L. Zhang, Z. Zhang, F. Wu, D. Wang, R. Gogna, S. Hou, K. Watanabe, T. Taniguchi, K. Kulkarni, T. Kuo, S. R. Forrest, H. Deng, *Nat. Commun.* **2020**, *11*, 5888.
[239] L. Zhang, F. Wu, S. Hou, Z. Zhang, Y.-H. Chou, K. Watanabe, T. Taniguchi, S. R. Forrest, H. Deng, *Nature* **2021**, *591*, 61.
[240] M. Amani, D.-H. Lien, D. Kiriya, J. Xiao, A. Azcatl, J. Noh, S. R. Madhvapathy, R. Addou, S. Kc, M. Dubey, K. Cho, R. M. Wallace, S.-C. Lee, J.-H. He, J. W. Ager, X. Zhang, E. Yablonovitch, A. Javey, *Science* **2015**, *350*, 1065.
[241] H. Kim, G. H. Ahn, J. Cho, M. Amani, J. P. Mastandrea, C. K. Groschner, D.-H. Lien, Y. Zhao, J. W. Ager, M. C. Scott, D. C. Chrzan, A. Javey, *Sci. Adv.* **2019**, *5*, eaau4728.
[242] J. Mork, K. Yvind, *Optica* **2020**, *7*, 1641.
[243] B. E. A. Saleh, M. C. Teich, *Proc. IEEE* **1992**, *80*, 451.
[244] S. Machida, Y. Yamamoto, Y. Itaya, *Phys. Rev. Lett.* **1987**, *58*, 1000.
[245] Y. Yamamoto, S. Machida, *Phys. Rev. A* **1987**, *35*, 5114.
[246] S. Machida, Y. Yamamoto, *Phys. Rev. Lett.* **1988**, *60*, 792.
[247] W. H. Richardson, S. Machida, Y. Yamamoto, *Phys. Rev. Lett.* **1991**, *66*, 2867.
[248] J. Kaiser, C. Degen, W. Elsässer, *Opt. Lett.* **2001**, *26*, 1720.
[249] R. Masuyama, A. Higashi, K. Tanaka, Y. Kadoya, M. Yamanishi, *Appl. Phys. Lett.* **2003**, *83*, 1113.
[250] P. Gallion, F. Jérémie, J. L. Vey, *Opt. Quantum Electron.* **1997**, *29*, 65.
[251] I. Maurin, I. Protsenko, J.-P. Hermier, A. Bramati, P. Grangier, E. Giacobino, *Phys. Rev. A* **2005**, *72*, 033823.
[252] S. Hu, S. M. Weiss, *ACS Photonics* **2016**, *3*, 1647.
[253] H. Choi, M. Heuck, D. Englund, *Phys. Rev. Lett.* **2017**, *118*, 223605.
[254] F. Wang, R. E. Christiansen, Y. Yu, J. Mørk, O. Sigmund, *Appl. Phys. Lett.* **2018**, *113*, 241101.
[255] B. Romeira, A. Fiore, *IEEE J. Quantum Electron.* **2018**, *54*, 200412.
[256] J. B. Khurgin, G. Sun, *Nat. Photon.* **2014**, *8*, 468.
[257] H.-J. Briegel, W. Dür, J. I. Cirac, P. Zoller, *Phys. Rev. Lett.* **1998**, *81*, 5932.
[258] S. Aaronson, A. Arkhipov, *arXiv:1011.3245[quant-ph]*, **2010**.
[259] H. Wang, J. Qin, X. Ding, M.-C. Chen, S. Chen, X. You, Y.-M. He, X. Jiang, L. You, Z. Wang, C. Schneider, J. J. Renema, S. Höfling, C.-Y. Lu, J.-W. Pan, *Phys. Rev. Lett.* **2019**, *123*, 250503.
[260] A. Schlehahn, A. Thoma, P. Munnelly, M. Kamp, S. Höfling, T. Heindel, C. Schneider, S. Reitzenstein, *APL Photon.* **2016**, *1*, 011301.
[261] Y.-J. Wei, Y.-M. He, M.-C. Chen, Y.-N. Hu, Y. He, D. Wu, C. Schneider, M. Kamp, S. Höfling, C.-Y. Lu, J.-W. Pan, *Nano Lett.* **2014**, *14*, 6515.
[262] N. Somaschi, V. Giesz, L. D. Santis, J. C. Loredo, M. P. Almeida, G. Hornecker, S. L. Portalupi, T. Grange, C. Antón, J. Demory, C. Gómez, I. Sagnes, N. D. Lanzillotti-Kimura, A. Lemaítre, A. Auffeves, A. G. White, L. Lanco, P. Senellart, *Nat. Photonics* **2016**, *10*, 340.
[263] S. Kreinberg, T. Grbešić, M. Strauß, A. Carmele, M. Emmerling, C. Schneider, S. Höfling, X. Porte, S. Reitzenstein, *Light: Sci. Appl.* **2018**, *7*, 1.
[264] P. Munnelly, T. Heindel, A. Thoma, M. Kamp, S. Höfling, C. Schneider, S. Reitzenstein, *ACS Photon.* **2017**, *4*, 790.
[265] X. Ding, Y. He, Z.-C. Duan, N. Gregersen, M.-C. Chen, S. Unsleber, S. Maier, C. Schneider, M. Kamp, S. Höfling, C.-Y. Lu, J.-W. Pan, *Phys. Rev. Lett.* **2016**, *116*, 020401.
[266] E. Stock, F. Albert, C. Hopfmann, M. Lermer, C. Schneider, S. Höfling, A. Forchel, M. Kamp, S. Reitzenstein, *Adv. Mater.* **2012**, *25*, 707.
[267] P. Munnelly, T. Heindel, M. M. Karow, S. Höfling, M. Kamp, C. Schneider, S. Reitzenstein, *IEEE J. Sel. Top. Quantum Electron.* **2015**, *21*, 681.
[268] Y.-R. Nowicki-Bringuier, J. Claudon, C. Böckler, S. Reitzenstein, M. Kamp, A. Morand, A. Forchel, J. M. Gérard, *Opt. Express* **2007**, *15*, 17291.
[269] P. Jaffrennou, J. Claudon, M. Bazin, N. S. Malik, S. Reitzenstein, L. Worschech, M. Kamp, A. Forchel, J.-M. Gérard, *Appl. Phys. Lett.* **2010**, *96*, 071103.
[270] P. R. Prucnal, B. J. Shastri, T. Ferreira Lima, M. A. Nahmias, A. N. Tait, *Adv. Opt. Photonics* **2016**, *8*, 228.
[271] M. Miscuglio, G. C. Adam, D. Kuzum, V. J. Sorger, *APL Mater.* **2019**, *7*, 100903.
[272] R. Amin, J. K. George, S. Sun, T. FerreiraLima, A. N. Tait, J. B. Khurgin, M. Miscuglio, B. J. Shastri, P. R. Prucnal, T. El-Ghazawi, V. J. Sorger, *APL Mater.* **2019**, *7*, 081112.

[273] A. N. Tait, T. de Ferreira Lima, M. A. Nahmias, H. B. Miller, H.-T. Peng, B. J. Shastri, P. R. Prucnal, *Phys. Rev. Appl.* **2019**, *11*, 064043.
[274] Y. Zuo, B. Li, Y. Zhao, Y. Jiang, Y. C. Chen, P. Chen, G. B. Jo, J. Liu, S. Du, *Optica* **2019**, *6*, 1132.
[275] D. Brunner, I. Fischer, *Opt. Lett.* **2015**, *40*, 3854.
[276] T. Rasmussen, Y. Yu, J. Mork, *Opt. Lett.* **2020**, *45*, 3844.
[277] K. Vandoorne, W. Dierckx, B. Schrauwen, D. Verstraeten, R. Baets, P. Bienstman, J. Van Campenhout, *Opt. Express* **2008**, *16*, 11182.
[278] K. Vandoorne, P. Mechet, T. Van Vaerenbergh, M. Fiers, G. Morthier, D. Verstraeten, B. Schrauwen, J. Dambre, P. Bienstman, *Nat. Commun.* **2014**, *5*, 1.
[279] T. Heuser, J. Grose, S. Holzinger, M. M. Sommer, S. Reitzenstein, *IEEE J. Sel. Top. Quantum Electron.* **2020**, *26*, 1900109.

Hui Deng received her Ph.D. from Stanford University in 2006. After a postdoctoral position at the California Institute of Technology, she joined the faculty of University of Michigan, Ann Arbor, in 2008, where she is currently a full professor. Her current research interests include light-matter interactions and phase transition physics in micro- and nano-photonic structures and van der Waals materials. H. Deng is a Fellow of the American Physical Society and the Optical Society of America.

Gian Luca Lippi received his Ph.D. in Physics from Bryn Mawr College (USA) in 1990. After a Humboldt-Fellowship Post-Doc at the University of Münster (Germany), and positions at the Université de Nice-Sophia Antipolis, he is currently Distinguished Professor at the Université Côte d'Azur. His current research interests revolve around experiments and models in the physics and dynamics of micro- and nanolasers, and biophotonics. G.L. Lippi is a member of the Optical Society of America and former director of two doctoral schools.

Jesper Mork received his Ph.D. in Applied Mathematical Physics from The Technical University of Denmark in 1988. Since 2002, he has been full professor at the Department of Photonics Engineering. His current research interests revolve around light–matter interaction in nanophotonic structures, including nanolasers, de-coherence in cavity QED, quantum noise and nonlinear dynamics. J. Mork is a Fellow of the Optical Society of America and is director of a newly established Center for Nanophotonics - NanoPhoton.

Jan Wiersig received his Ph.D. from the University of Bremen in 1998. He was a postdoctoral researcher at the Queen Mary and Westfield College in London, at the Max Planck Institute for the Physics of Complex Systems in Dresden, and at the University of Bremen. In 2008, he became a full Professor at the Otto von Guericke University Magdeburg. His current research interests include light–matter interaction in semiconductor micro- and nanostructures, wave chaos and non-Hermitian effects in optical microcavities.

Stephan Reitzenstein received his Ph.D. degree in physics (summa cum laude) from the University of Würzburg, Germany, in 2005. In 2010, he habilitated with studies regarding optical properties of low-dimensional semiconductor systems. Since September 2011, he has been a full Professor at the Technical University of Berlin, Germany, holds the Chair of Optoelectronics and Quantum Devices, and is director of the Center of Nanophotonics. His research interests are in the area of micro-/nanolasers and quantum optics in semiconductor nanostructures. S. Reitzenstein is member of the German Physical Society where he is presently the spokesman of the Semiconductor Division.